HACON - A Program for Simulation of Temperature and Stress in Hardening Concrete

Dahlblom, Ola; Lindemann, Jonas

2000

Document Version:
Publisher's PDF, also known as Version of record

LUND UNIVERSITY

HACON

A PROGRAM FOR SIMULATION OF TEMPERATURE AND STRESS IN HARDENING CONCRETE

OLA DAHLBLOM and JONAS LINDEMANN

Structural Mechanics

Structural Mechanics

ISRN LUTVDG/TVSM--00/3057--SE (1-66)
ISSN 0281-6679

HACON

A PROGRAM FOR SIMULATION OF TEMPERATURE AND STRESS IN HARDENING CONCRETE

OLA DAHLBLOM and JONAS LINDEMANN

Printed by KFS i Lund AB, Lund, Sweden, May 2000.

For information, address:
Division of Structural Mechanics, LTH, Lund University, Box 118, SE-221 00 Lund, Sweden.
Homepage: http://www.byggmek.lth.se

Preface

The computer program described in the present report has been developed as a joint project between the Division of Structural Mechanics at Lund University and Vattenfall Utveckling AB. The project was initiated by Jan Alemo in 1987. During the late 80s and early 90s Ola Dahlblom performed the program development and wrote the description of theory which the computer code is based on. During recent years a major revision of the computer program has been performed, including development of a graphical user interface and also some development of the modelling code. This revision was performed by Ola Dahlblom and Jonas Lindemann.

Lund in May 2000

Ola Dahlblom Jonas Lindemann

Contents

Chapter 1

INTRODUCTION

1.1 General remarks

The service life of concrete structures is to a great extent influenced by crack development.

Owing to chemical reactions, heat is developed in hardening concrete. This normally yields a temperature increase and thermal expansion. Since displacement is often prevented by an existing structure, e.g. when an old concrete structure is repaired, tensile stress and crack development may occur when the temperature decreases after the hardening. Another source of crack development is nonuniform distribution of temperature and thermal strain in hardening concrete structures.

A crucial point in the design of massive concrete structures is to avoid crack development during hardening. To do this, different methods are used, e.g. use of low heat cement, limitation of casting stages, cooling of the concrete before casting, cooling of the concrete structure with internal pipes, etc. In the absence of suitable computer programs the effect of this type of action has in the past been estimated very roughly. To facilitate more accurate prediction of the effect, a computer program for simulation of temperature and stress in hardening concrete structures has been developed. The present program is called HACON and is a further development of the programs HACON-T [8], HACON-S [9] and HACON-H [10]. A brief description of the program HACON is given below.

1.2 Characteristics of computer program

Some characteristics of the computer program are mentioned below.

- The finite element method is applied.
- Two-dimensional and axisymmetric problems can be handled.
- The heat development of the cement is described as a function of the temperature and the degree of hydration.

- Heat exchange with an unbounded region of e.g. rock is considered, using finite elements.
- The finite element model can be extended during the analysis to consider casting stages performed at different points of time.
- Variations in the environmental temperature and the removal of formwork and insulation can be considered.
- The temperature or generated heat can be prescribed at specific points to take into consideration the effect of cooling pipes or heating cables.
- In the stress analysis the development of material properties during hardening is considered.
- The constitutive equations take into account creep, stress induced thermal strain, autogeneous shrinkage and crack developmet.

Input data to the program is defined interactively and mesh generation is included.

Output data from the program is stored in a file, which is interpreted by a special purpose post-processor. Distribution of temperature, degree of hydration and equivalent maturity time are presented by colour or iso-lines. The history of the temperature at a specified point and the mean, maximum and minimum temperature, in a specified region are shown in diagrams. Displacements are illustrated by showing a deformed finite element mesh. Magnitude and direction of principal stresses are shown by arrows. Distribution of maximum principal stress, strength and stress-strength ratio are presented by colour. The history of stress, strength and stress-strength ratio is shown in diagrams.

1.3 Summary of the report contents

In Chapters 2-4 a description of the theory which the program is based on is given.

In Chapter 5 the computer program is described briefly.

1.4 Notations

The notations are explained in the text where they first appear. They are also listed in Appendix A.

References to literature are quoted in the text by numbers in square brackets, [ ]. The references are given in alphabetical order in Appendix C.

Equations are, in general, written in component form and unless otherwise indicated, the summation convention is applied, see e.g. Malvern [24].

A component of a vector is indicated by using indices, e.g. q_i. To make a distinction between the vector itself and its components, vectors are denoted by boldface letters, e.g. $\mathbf{q}$. The time derivative is denoted by a dot over the variable considered, e.g. $\dot{T}$.

Chapter 2

PROPERTIES OF HARDENING CONCRETE

2.1 Introduction

Theoretical simulation of displacements and stresses in hardening concrete structures require a proper material description. The material model, which will be described below, aims to be general enough to reflect the phenomena of interest, without being more complicated than necessary. Influence of hardening on the material properties is taken into account. In the present work, the concrete is assumed not to be affected by drying. Therefore, influence of drying on the material properties is not considered. Since the tensile strength of concrete is much lower than the compressive strength, a common situation is that the tensile strength is exceeded, while the maximum compressive stress is well below the compressive strength. For convenience, compression failure is therefore not included in the present model.

Heat development and development of material properties are dependent on the hydration process. Therefore a description of this process is given below.

2.2 Hydration of concrete

After casting, the strength of the concrete develops during the hydration process, which consists of several simultaneous chemical reactions. To obtain a measure of how far the reactions have developed, the quantity degree of hydration α is introduced. Several definitions of this quantity have been proposed, see Byfors [5].

In the present work, the degree of hydration α is defined as the quantity of heat developed W_c, divided by the quantity of heat developed at complete hydration of the cement W_{c0}, i.e.

$$\alpha = \frac{W_c}{W_{c0}} \tag{2.1}$$

Since the hydration process is dependent on temperature, it is reasonable to

introduce the quantity equivalent maturity time t_e, which facilitates the comparison of hydration processes during different thermal conditions. The equivalent maturity time t_e is defined by the integral

$$t_e = \int_0^t \frac{f(T)}{f(T_r)} d\tau \tag{2.2}$$

where $f(T)$ is a maturity function and T_r is a reference temperature, chosen as $T_r = 293K$ $(20°C)$. Several maturity functions have been proposed, see Byfors [5] for a review. Freiesleben Hansen and Pedersen [14] proposed a maturity function based on the Arrhenius equation for thermal activation, i.e.

$$f(T) = k e^{-\frac{\theta}{T}} \tag{2.3}$$

In Eq. (2.3) k is a proportionality constant and θ is the activation energy divided by the universal gas constant. Substitution of Eq. (2.3) into Eq. (2.2) yields

$$t_e = \int_0^t e^{\theta(\frac{1}{T_r} - \frac{1}{T})} d\tau \tag{2.4}$$

Use of Eq. (2.4) with the assumption of temperature dependency of θ, has shown a good correlation between the equivalent maturity time and the compressive concrete strength, see Freiesleben Hansen and Pedersen [14] and Byfors [5]. In the present work Eq. (2.4) is used, with the quantity θ given by

$$\theta = \theta_0 \left(\frac{T_r - T_a}{T - T_a} \right)^{\kappa_0} \tag{2.5}$$

as proposed by Jonasson [20]. In Eq. (2.5), θ_0 and κ_0 are material parameters obtained experimentally, and T_a is a constant chosen as $T_a = 263K$ $(-10°C)$.

The quantity of generated heat per mass unit of cement W_c is related to the degree of hydration α by Eq. (2.1). To obtain an expression for how the generated heat is related to the equivalent maturity time t_e, a relation between α and t_e is required. In the present work the relation proposed by Jonasson [20] is adopted, i.e.

$$\alpha = e^{-\lambda_1 (\ln(1 + \frac{t_e}{t_1}))^{-\kappa_1}} \tag{2.6}$$

where λ_1, t_1 and κ_1 are material parameters obtained experimentally.

In Appendix B a description of a method for determination of the material parameters in Eqs. (2.5) and (2.6) from measurements using an insulated curing box is given.

In a concrete structure the generated heat per volume unit is of interest. Therefore, the generated heat per mass unit of cement is multiplied by the cement content C, i.e. the generated heat per volume unit of concrete W is given by

$$W = C W_c \tag{2.7}$$

Substitution of Eq. (2.1) into Eq. (2.7) yields

$$W = CW_{c0}\alpha \tag{2.8}$$

In the finite element equations, the time derivative of W will be used. Differentiation of Eq. (2.8) yields

$$Q = \frac{dW}{dt} = CW_{c0}\frac{d\alpha}{dt_e}\frac{dt_e}{dt} \tag{2.9}$$

where, according to Eqs. (2.6) and (2.4)

$$\frac{d\alpha}{dt_e} = \alpha\frac{\lambda_1\kappa_1}{t_1+t_e}\left(\ln\left(1+\frac{t_e}{t_1}\right)\right)^{-\kappa_1-1} \tag{2.10}$$

$$\frac{dt_e}{dt} = e^{\theta\left(\frac{1}{T_r}-\frac{1}{T}\right)} \tag{2.11}$$

2.3 Compressive strength

As mentioned above, compression failure is not included in the model. It is, however, common to relate some material properties of hardening concrete to the compressive strength. Therefore, a description of this is given below.

The compressive strength f_{c0}, after hardening for a reference time $t_r = 672h$ (28d), at a reference temperature $T_r = 293K$ (20^0C), is often used as a measure of the quality of the concrete. The strength f_{c0} depends mainly on the water-cement ratio w_0/C.

For Swedish standard cement Ref. [4] gives a diagram showing the relation between water-cement ratio w_0/C and compressive strength f_{c0}. A fair representation of the relation can be described by the expression

$$f_{c0} = f_{c1} + \frac{f_{c2}}{(w_0/C)} \tag{2.12}$$

where the parameters have the values $f_{c1} = -4.7MPa$ and $f_{c2} = 27.5MPa$.

During hardening the compressive strength f_c is assumed to develop according to a relation described by Byfors [5], i.e.

$$f_c = \eta_c f_{c0} \tag{2.13}$$

where

$$\eta_c = \frac{a_{1c}\left(\frac{t_e}{t_r}\right)^{b_{1c}}}{1+\frac{a_{1c}}{a_{2c}}\left(\frac{t_e}{t_r}\right)^{(b_{1c}-b_{2c})}} \tag{2.14}$$

and the parameters a_{1c}, b_{1c}, a_{2c} and b_{2c} depend on the cement type and the concrete composition. In absence of detailed experimental data on the concrete in question, the parameters may, on the basis of experimental data presented by Byfors [5], be chosen as $a_{1c} = 10^{(3.4-1.1W_0/C)}$, $b_{1c} = 2.0$, $a_{2c} = 1.0$, and $b_{2c} = 0.14$.

2.4 Elastic strain

During hardening, the elasticity properties change. It is, however, reasonable to assume that the deformation of concrete which is subjected to load is maintained during hardening. This is because chemical reactions cause development of the internal material structure, and the new connection produced can be expected to be free from stress and not carry the previously applied load. However, these connections yield an increased material stiffness. Unloading of the material will therefore show an irreversible strain caused by hardening of loaded concrete. Assuming isotropy, the elastic strain rate $\dot{\varepsilon}^e$ is thus related to the stress rate $\dot{\sigma}$ by the generalized Hooke's law

$$\dot{\varepsilon}^e_{ij} = C^e_{ijkm}\dot{\sigma}_{km} \tag{2.15}$$

where C^e is the isotropic compliance tensor, given by

$$C^e_{ijkm} = \rho_e\delta_{ij}\delta_{km} + \kappa_e\left(\delta_{ik}\delta_{jm} + \delta_{im}\delta_{jk}\right) \tag{2.16}$$

Here δ_{ij} is Kronecker's delta and ρ_e and k_e are elastic parameters, related to the elastic modulus E and Poisson's ratio ν by

$$\rho_e = -\frac{\nu}{E} \tag{2.17}$$

$$\kappa_e = \frac{1+\nu}{2E} \tag{2.18}$$

The growth of the elastic modulus E during hardening may be described in the same manner as the development of the compressive strength f_c has been described by Byfors [5], i.e.

$$E = \eta_E E_0 \tag{2.19}$$

where

$$\eta = \frac{a_{1E}\left(\frac{t_e}{t_r}\right)^{b_{1E}}}{1+\frac{a_{1E}}{a_{2E}}\left(\frac{t_e}{t_r}\right)^{(b_{1E}-b_{2E})}} \tag{2.20}$$

and E_0 is the elastic modulus at time $t_e = t_r$. The parameters a_{1E}, b_{1E}, a_{2E} and b_{2E} depend on the cement type and the concrete composition. Eq. (2.19), with parameters chosen as $a_{1E} = 10^{(8.0-2.0W_0/C)}$, $b_{1E} = 4.0$, $a_{2E} = 1.0$, and $b_{2E} = 0.1$, is compared with experimental data by Byfors [5] in Fig. 2.1. In accordance with the experimental data, the value of E_0 has been chosen as $38.0GPa$, $38.0GPa$ and $31.0GPa$ for the water-cement ratios 0.40, 0.58, and 1.00, respectively. To get an estimation of the value of E_0 in Eq. (2.19) one may use the relation

$$E_0 = E_1\sqrt{\frac{f_{c0}}{f_r}} \tag{2.21}$$

where $E_1 = 6.0GPa$ and f_r is a reference value, chosen as $f_r = 1.0MPa$.

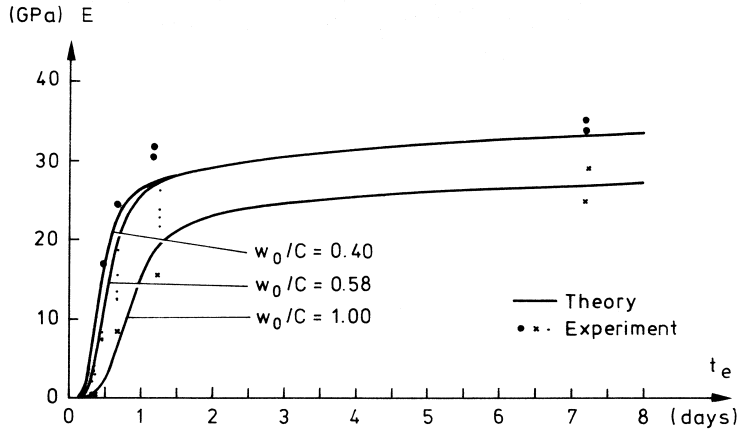

Figure 2.1: Comparison between Eq. (2.19) and experimental data according to Byfors [5].

According to experimental data by Byfors [5] the value of Poisson's ratio decreases rapidly at a very early age, and then increases. This behaviour may be described by the relation

$$\nu = \nu_1 e^{-\alpha_{1\nu}\left(\frac{t_e}{t_r}\right)} + \nu_2 \left(1 - e^{-\alpha_{1\nu}\left(\frac{t_e}{t_r}\right)}\right) \tag{2.22}$$

where ν_1 and ν_2 are the initial and final values of ν, respectively, and $\alpha_{1\nu}$ and $\alpha_{2\nu}$ ($\alpha_{1\nu} > \alpha_{2\nu}$) are parameters which express the influence of hardening. In Fig. 2.2 Eq. (2.22), with $\nu_1 = 0.5$, $\nu_2 = 0.25$, $\alpha_{1\nu} = 150$, and $\alpha_{2\nu} = 40$, is illustrated and compared with experimental data according to Byfors [5].

2.5 Thermal strain

When the temperature of concrete is raised by the rate $\dot{T}$, thermal strain develops with the rate $\alpha_T \delta_{ij} \dot{T}$, where α_T is the coefficient of thermal expansion. The value of α_T is dependent on the concrete composition and is reducing during the first few hours after casting, see Byfors [5]. A typical value of α_T is $10{\cdot}10^{-6}K^{-1}$.

According to experimental results by e.g. Löfquist [23] and Emborg [13], the thermal strain is only partly recovered when the temperature is decreased. The thermal strain rate $\dot{\varepsilon}^T$can thus be expressed as

$$\dot{\varepsilon}^T_{ij} = \alpha_T \left(r_T + \beta_T \left(1 - r_T\right)\right) \delta_{ij} \dot{T} \tag{2.23}$$

where r_T is a parameter indicating to what extent the thermal strain is recoverable and β_T is a parameter with the value 1 when the temperature increases to a level not previously attained, and 0 in other cases. According to the data by Löfquist [23] and Emborg [13] the parameter r_T has a value in the range 0.6 - 1.0, and a typical value is $r_T = 0.8$.

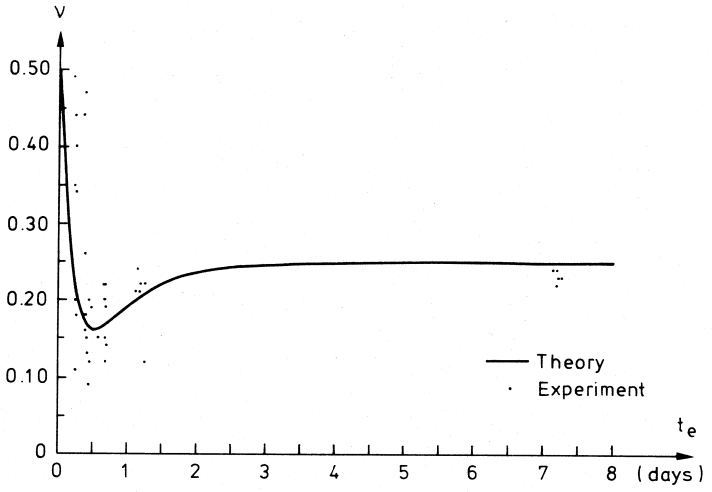

Figure 2.2: Comparison between Eq. (2.22) and experimental data according to Byfors [5].

2.6 Stress induced thermal strain

When the temperature of a concrete specimen exposed to external load is raised, the observed deformation differs from the sum of the deformation of a loaded specimen at constant temperature and the thermal expansion of a non-loaded specimen. The excess deformation is often called transitional thermal creep, and is sometimes referred to as stress induced thermal stain. For temperatures below 100^0C, the phenomenon has been observed by e.g. Hansen and Eriksson [15], Illston and Sanders [18], [19] and Parrott [28]. Khoury et al. [21] have made an excellent review of experimental observations in this area. Important characteristics are that the strain develops rapidly after increase of temperature to a level not previously attained and that it is irrecoverable. The magnitude of the strain is proportional to the stress and to the temperature change and may be regarded as unaffected by maturity. The rate of the stress induced strain $\dot{\varepsilon}^{T\sigma}$, as proposed by Thelandersson [34], can be assumed to be given by the relation

$$\dot{\varepsilon}_{ij}^{T\sigma} = \beta_{T\sigma} C_{ijkm}^{T\sigma} \sigma_{km} \dot{T} \tag{2.24}$$

where $C^{T\sigma}$ is a tensor which, assuming isotropy, can be expressed as

$$C_{ijkm}^{T\sigma} = \rho_{T\sigma} \delta_{ij} \delta_{km} + \kappa_{T\sigma} \left(\delta_{ik} \delta_{jm} + \delta_{im} \delta_{jk} \right) \tag{2.25}$$

In Eq. (2.24) σ is the stress, $\dot{T}$ is the time derivative of temperature, and $\beta_{T\sigma}$ is a parameter with the value 1 when the temperature increases to a level not previously attained, and 0 in other cases. In Eq. (2.25), $\rho_{T\sigma}$ and $\kappa_{T\sigma}$ are material parameters, which in analogy with Eqs. (2.19) and (2.20) can be expressed as

$$\rho_{T\sigma} = -\frac{\nu_{T\sigma}}{E_{T\sigma}} \tag{2.26}$$

$$\kappa_{T\sigma} = \frac{1 + \nu_{T\sigma}}{2E_{T\sigma}} \tag{2.27}$$

According to the data given in Refs. [18], [28] and [21], $E_{T\sigma}$ varies between 0.5 and $4.0TPaK$ and a typical value is $2.0TPaK$. The value of $\nu_{T\sigma}$ cannot be obtained from the data in these references, but data for concrete heated above $100°C$, given by Thelandersson [34], yields $\nu_{T\sigma} = 0.29$, i.e. about the same as the value of Poisson's ratio ν for hardened concrete. In absence of detailed experimental data, $\nu_{T\sigma}$ may be assumed to have a value in the range $0.25 - 0.30$.

2.7 Autogeneous shrinkage

In concrete with a low water-cement ratio the chemical reactions during hardening result in a decrease in humidity, so-called self-desiccation. This decrease in humidity yields strains commonly referred to as autogeneous shrinkage. The development of autogeneous shrinkage starts when the capillary water has been consumed due to the hydration. The autogeneous shrinkage ε_a is, as proposed by Auperin et al. [2], assumed to be given by the expression

$$\varepsilon^a_{ij} = \varepsilon_{a0} e^{-(\frac{t_e - t_a}{t_2})^{-\kappa_2}} \delta_{ij}; \qquad t_e \geq t_a \tag{2.28}$$

where ε_{a0} is the final autogeneous shrinkage, t_a is the maturity at start of autogeneous shrinkage and t_2 and κ_2 are development parameters for the autogeneous shrinkage.

Equation (2.28) with the parameters chosen as $\varepsilon_{a0} = -0.7 \cdot 10^{-4}$, $t_a = 50h$, $t_2 = 400h$ and $\kappa_2 = 1.1$ is illustrated in Fig. (2.3).

2.8 Creep strain

Time dependent strain, often referred to as creep, may be assumed to be proportional to the stress. For a constant uniaxial stress σ the creep strain ε_c can be written

$$\varepsilon_c = C\sigma \tag{2.29}$$

where C is the creep compliance, which is dependent on time t, loading time t', and concrete composition. The creep compliance may be expressed as

$$C = \frac{1}{E}\phi_0\phi'_t\phi_t \tag{2.30}$$

in which E is the elastic modulus and ϕ_0 and ϕ_t are parameters, whose values can be obtained from diagrams given in Ref. [4]. The relations can, with good agreement, be described by the expressions

$$\phi_0 = \phi_{01}\frac{w_0}{C} - \phi_{02} \tag{2.31}$$

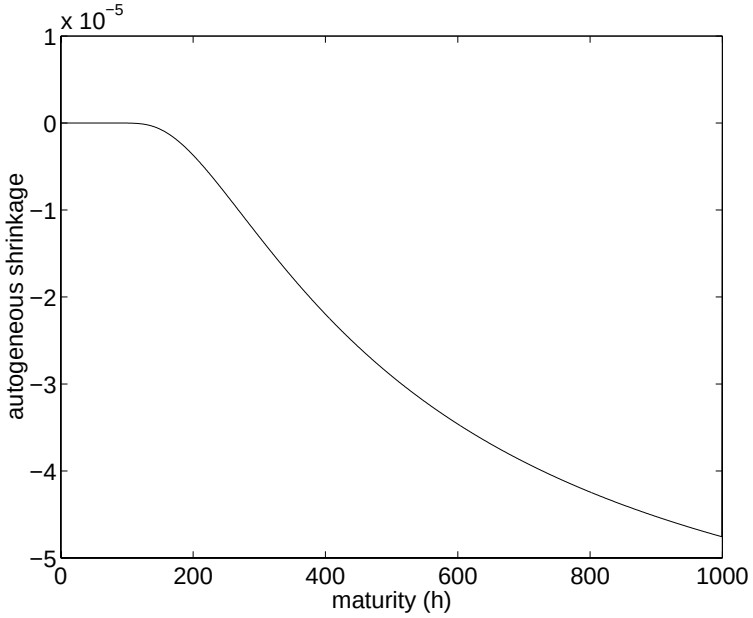

Figure 2.3: Illustration of Eq. (2.28).

$$\phi_t = \sum_{n=1}^{N} \phi_n \left[1 - e^{-\frac{t-t'}{\tau_n}}\right] \tag{2.32}$$

where Eq. (2.32) is known as a Dirichlet series. The parameters may be chosen as $\phi_{01} = 3.2$, $\phi_{02} = 0.3, N = 5$, $\tau_1 = 10^4 s$, $\tau_2 = 10^5 s$, $\tau_3 = 10^6 s$, $\tau_4 = 10^7 s$, $\tau_5 = 10^8 s$, $\phi_1 = 0.06$, $\phi_2 = 0.03$, $\phi_3 = 0.20$, $\phi_4 = 0.52$ and $\phi_5 = 0.15$. The parameter ϕ_t considers the influence of the concrete age at loading. This influence may be described by the relation

$$\phi_t' = \left(\frac{t_e}{t_r}\right)^{-\phi_{t1}'} \tag{2.33}$$

This expression, with $\phi_{t1}' = 0.27$, is illustrated in Fig. 2.4. In the figure data from several experiments as compiled by Parrot [29] is also shown (from Byfors [5]). A comparison with the curve given in Ref. [4] is also provided.

Adopting the principle of superposition, which means that the creep strain due to a varying stress is equal to the sum of the creep strains due to stress increments applied at different times t', see e.g. Bazant [3], the creep strain may be written

$$\varepsilon_c = \int_0^t C \frac{d\sigma}{dt'} dt' \tag{2.34}$$

Assuming isotropy, the following generalization of Eq. (2.34), see e.g. Bazant

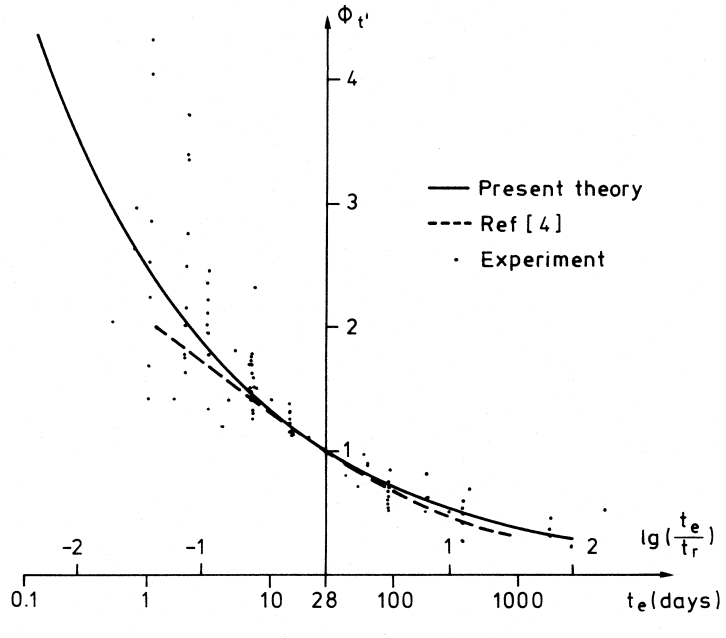

Figure 2.4: Comparison between theory and experimental data.

[3], can be used

$$\varepsilon_{ij}^{c} = \sum_{n=1}^{N} \int_{0}^{t} C_{ijkm}^{cn} \left[1 - e^{-\frac{t-t'}{\tau_n}}\right] \frac{d\sigma_{km}}{dt'} dt' \tag{2.35}$$

where the creep compliance tensor $\mathbf{C}^{cn}$can be expressed in a way similar to the elastic compliance tensor in Eq. (2.18), i.e.

$$C_{ijkm}^{cn} = \rho_{cn}\delta_{ij}\delta_{km} + \kappa_{cn}\left(\delta_{ik}\delta_{jm} + \delta_{im}\delta_{jk}\right) \tag{2.36}$$

in which ρ_{cn} and κ_{cn} are creep compliance parameters which, analogously to Eqs. (2.21) and (2.22) can be expressed as

$$\rho_{cn} = -\frac{\nu_{cn}}{E_{cn}} \tag{2.37}$$

$$\kappa_{cn} = \frac{1 + \nu_{cn}}{2E_{cn}} \tag{2.38}$$

where E_{cn} is given by the relations

$$\begin{aligned} E_{cn} &= \tfrac{E}{\phi_0 \phi_t' \phi_n}; \quad n = 1 \\ E_{cn} &= \tfrac{E_0}{\phi_0 \phi_t' \phi_n}; \quad n \geq 2 \end{aligned} \tag{2.39}$$

and ν_{cn} are quantities analogous to Poisson's ratio ν. To avoid great influence at a late stage, from stress variations at an early stage, E_{cn} has for $n \geq 2$ been assumed

to be proportional to E_0 instead of E. In absence of detailed experimental results one may assume that $\nu_{cn} = \nu$, see e.g. Anderson [1].

The time derivative of the creep strain ε^c_{ij}, according to Eq. (2.35) is given by

$$\dot{\varepsilon}^c_{ij} = \sum_{n=1}^{N} \frac{1}{\tau_n} e^{-\frac{t}{\tau_n}} \gamma^n_{ij} \tag{2.40}$$

where the quantities γ_{ij} express the history of the material and are given by

$$\gamma^n_{ij} = \int_0^t C^{cn}_{ijkm} e^{\frac{t'}{\tau_n}} \frac{d\sigma_{km}}{dt'} dt' \tag{2.41}$$

It may be observed that when the creep strain rate at time $t + \Delta t$ is to be computed, the integral of Eq. (2.41) has to be evaluated only from time t to time $t + \Delta t$, if the value of the integral at time t is known. This means that the stress history before time t need not be available when the creep strain rate at time $t + \Delta t$ is to be computed.

2.9 Fracturing strain

The fictitious crack model according to Hillerborg et al. [16], [17], [26] is based on the fact that when a specimen is loaded in tension, fracture is localized to a thin zone. The deformation caused by fracture in this zone is modelled by a fictitious crack whose width represents the total fracturing deformation in the zone. The material outside the fracture zone is assumed to be unaffected by cracking.

A smeared crack approach based on the fictitious crack model has been proposed by Ottosen and Dahlblom [27], [11], [7]. In the present model the concept is modified to consider development of properties during hardening.

Crack development is assumed to start when the maximum principal stress reaches the uniaxial tensile strength f_t, which grows during hardening.

The development of the tensile strength f_t may be described in analogy with the growth of the elastic modulus as described above, i.e.

$$f_t = \eta_t f_{t0} \tag{2.42}$$

where

$$\eta_t = \frac{a_{1t} \left(\frac{t_e}{t_r}\right)^{b_{1t}}}{1 + \frac{a_{1t}}{a_{2t}} \left(\frac{t_e}{t_r}\right)^{(b_{1t} - b_{2t})}} \tag{2.43}$$

and f_{t0} is the tensile strength at time $t_e = t_r$. An estimation of the value of f_{t0} can be obtained by the relation

$$f_{t0} = f_{t1} \left(\frac{f_{c0}}{f_r}\right)^{\frac{2}{3}} \tag{2.44}$$

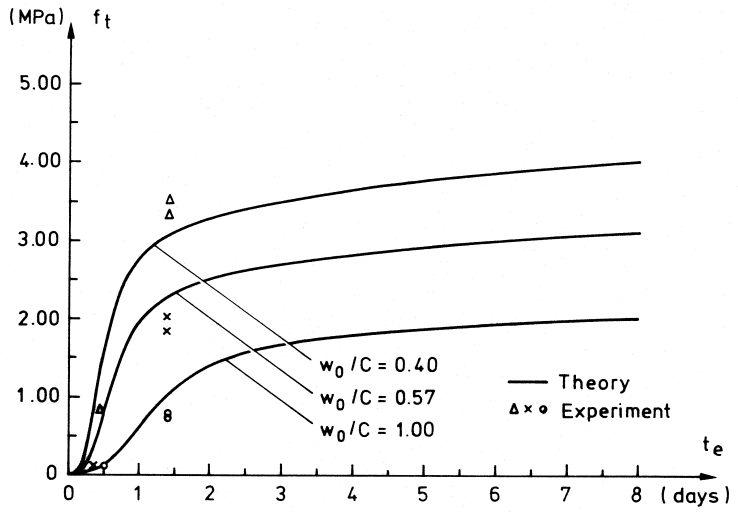

Figure 2.5: Comparison between Eq. (2.42) and experimental data according to Byfors [5].

where f_r is a reference value chosen as $f_r = 1.0MPa$. Eq. (2.42) is illustrated in Fig. 2.5, with the parameters chosen as $a_{1t} = 10^{\left(6.0-2.0\frac{w_0}{C}\right)}$, $b_{1t} = 3.0$, $a_{2t} = 1.0$, $b_{2t} = 0.14$, and $f_{t1} = 0.3MPa$. Experimental data representing the tensile strength obtained by Byfors [5] in splitting tests is also shown in the figure.

The crack plane of the first crack is assumed to be normal to the direction of the maximum principal stress. A possible second crack is assumed to develop perpendicular to the first crack, if the normal stress in that direction also reaches the tensile strength. Likewise a third crack may develop perpendicular to the existing two cracks.

For convenience, a local coordinate system is introduced, where the $\bar{x}_1$-axis is normal to the plane of the first crack. If a second crack has occurred, the $\bar{x}_2$-axis is normal to the plane of that crack. The unit vectors $\bar{\mathbf{i}}_i$ in the local coordinate system are related to the unit vectors $\mathbf{i}_k$ in the global coordinate system by the relation

$$\bar{\mathbf{i}}_i = a_{ik}\mathbf{i}_k \tag{2.45}$$

where

$$a_{ik} = \cos\left(\bar{x}_i,\, x_k\right) \tag{2.46}$$

in which $\bar{x}_i$ and x_k denote local and global coordinates respectively. It may be noted that, in the present description of fracture, barred variables relate to the local coordinate system.

The stress $\bar{\sigma}_{\alpha\alpha}$ normal to the plane of crack No. α is assumed to decrease when the crack width $\bar{w}_\alpha$ increases. It should be noted that when α or β is used as tensor index, in this description, a specific component is assumed and that the summation convention is not applied for a repeated index α or β.

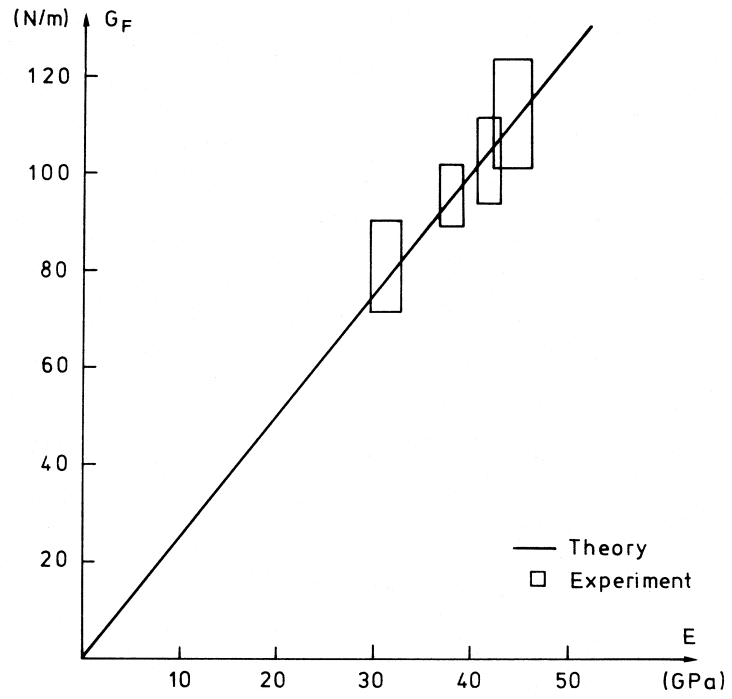

Figure 2.6: Comparison between Eq. (2.48) and experimental data by Petersson [31]

The energy G_F necessary to produce one unit area of crack is given by the integral

$$G_F = \int_0^{w_c} \bar{\sigma}_{\alpha\alpha} d\bar{w}_\alpha \tag{2.47}$$

where w_c is the crack width when the normal stress has dropped to zero. According to experimental results by Petersson [31], the fracture energy G_F of hardening concrete develops in the same way as the elastic modulus E. Thus, the fracture energy G_F may be described as

$$G_F = \eta_E G_{F0} \tag{2.48}$$

where G_{F0} is the fracture energy at time $t_e = t_r$. To get an estimation of the value of G_{F0} one may use the relation

$$G_{F0} = G_{F1} E_0 \tag{2.49}$$

where $G_{F1} = 2.5$ mm gives good agreement with experimental data according to Petersson [31], see Fig. 2.6.

The stress $\bar{\sigma}_{\alpha\alpha}$ is for the sake of simplicity assumed to be a linear function of $\bar{w}_\alpha$, i.e.

$$\bar{\sigma}_{\alpha\alpha} = f_t + N\bar{w}_\alpha \tag{2.50}$$

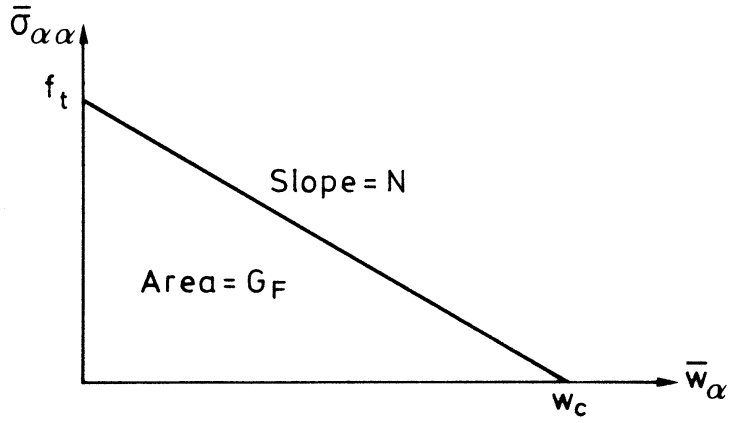

Figure 2.7: Relation of stress $\bar{\sigma}_{\alpha\alpha}$ and crack width $\bar{w}_\alpha$

where f_t is the uniaxial tensile strength and N is a proportionality factor ($N < 0$). The relation between stress $\bar{\sigma}_{\alpha\alpha}$ and crack width $\bar{w}_\alpha$ is illustrated in Fig. 2.7.

Eq. (2.50) and the fact that the normal stress is zero when the crack width is w_c yield

$$w_c = -\frac{f_t}{N} \tag{2.51}$$

Substitution of Eq. (2.50) into Eq. (2.47), evaluation of the integral and use of Eq. (2.51) results in

$$N = -\frac{f_t^2}{2G_F} \tag{2.52}$$

A fracturing strain tensor ε^f is introduced which represents the mean fracturing strain in a region which includes the discrete crack. The fracturing strain $\bar{\varepsilon}^f_{\alpha\alpha}$ normal to the plane of crack No. α is defined by

$$\bar{\varepsilon}^f_{\alpha\alpha} = \frac{\bar{w}_\alpha}{L_\alpha} \tag{2.53}$$

where L_α is an equivalent length associated with crack No. α which is related to the size of the finite element where the crack develops.

Substitution of Eq. (2.53) into Eq. (2.50) and differentiation with respect to time yields

$$\dot{\bar{\varepsilon}}^f_{\alpha\alpha} = J_\alpha \dot{\bar{\sigma}}_{\alpha\alpha} \tag{2.54}$$

where

$$J_\alpha = \frac{1}{NL_\alpha} \tag{2.55}$$

Eq. (2.55) is valid on condition that

$$\dot{\bar{w}}_\alpha > 0 \tag{2.56}$$

If this condition is not satisfied, i.e. unloading is taking place, the crack that has developed is assumed to be irrecoverable and the fracturing strain rate is assumed to be zero. This means that Eq. (2.54) is still valid, but now with J_α given by

$$J_\alpha = 0 \tag{2.57}$$

When a crack is fully developed, i.e. when $\bar{w}_\alpha > w_c$, the stress $\bar{\sigma}_{\alpha\alpha}$ is assumed to be zero. If Eq. (2.54) is applied in this situation the value of J_α is infinitely large.

As mentioned above, the fracture energy is given by Eq. (2.47), which means that the remaining fracture energy of a developing crack is changed by the rate $-\bar{\sigma}_{\alpha\alpha}\dot{\bar{w}}_\alpha$ when the rate of change in the crack width is $\dot{\bar{w}}_\alpha$. In hardening concrete it may be assumed that new connections develop in undamaged regions of fracturing concrete. The remaining fracture energy G_α is therefore assumed to increase by a fraction G_α/G_F of the increase of G_F, as described by Eq. (2.49). These assumptions lead to the following description of the rate of change of the remaining fracture energy $\dot{G}_\alpha$.

$$\dot{G}_\alpha = \tfrac{G_\alpha}{G_F}\dot{G}_F - \bar{\sigma}_{\alpha\alpha}\dot{\bar{w}}_\alpha; \quad \dot{\bar{w}}_\alpha > 0 \tag{2.58}$$

If a crack, fully or partly developed, is exposed to compressive stress, the hardening process may yield new connections even in damaged regions, since contact can be expected between particles on different sides of the crack plane. The remaining fracture energy G_α may therefore be assumed to increase by the same rate as the fracture energy G_F, i.e.

$$\dot{G}_\alpha = \dot{G}_F; \quad \bar{\sigma}_{\alpha\alpha} \leq 0, \dot{\bar{w}}_\alpha = 0 \tag{2.59}$$

For tensile stresses below the current tensile strength f_α linear interpolation between Eq. (2.58) and Eq. (2.59) may be applied, i.e. the rate of change of fracture energy is given by

$$\dot{G}_\alpha = \left(1 + \tfrac{\bar{\sigma}_{\alpha\alpha}}{f_\alpha}\left(\tfrac{G_\alpha}{G_F} - 1\right)\right)\dot{G}_F; \quad 0 \leq \bar{\sigma}_{\alpha\alpha} \leq f_\alpha, \ \dot{\bar{w}}_\alpha = 0 \tag{2.60}$$

where the tensile strength f_α is proportional to the square root of the remaining portion of the fracture energy, i.e.

$$f_\alpha = \sqrt{\frac{G_\alpha}{G_F}} f_t \tag{2.61}$$

Development of a crack will reduce the ability to transfer shear stresses across the crack plane. In analysis of fracture it is important, in addition to modelling the behaviour normal to a crack plane, to obtain a reasonable expression for the shear behaviour. A common way of handling the reduction of shear stiffness is simply to multiply the elastic shear modulus by a so-called shear retention factor, which has a constant value in the interval from 0 to 1. It is, however, not satisfactory to assume that the reduction of the shear stiffness is independent of the crack width.

It is reasonable to assume that the shear stiffness is reduced gradually as the crack width increases. Since the fracture is localized to a thin zone, the reduction of shear stiffness is related to this zone and the shear stiffness in the region outside the zone is unaffected by cracking. When a smeared crack approach is used, an effective shear modulus, representative of a region which includes the crack, is applied. The effective shear modulus depends on the shear stiffness of the fracture zone and also on the shear stiffness of the unaffected region outside the zone, and is therefore dependent on the size of the region considered. It is thus not acceptable to use a shear retention factor which is not related to the size of the region of which it is assumed to be representative. In experiments by Paulay and Loeber [30] relationships between shear stress and shear displacement at constant crack widths have been obtained. According to their results the shear displacement is more or less proportional to the shear stress and to the crack width. Based on these observations the shear displacement $\bar{w}^s_{\alpha\beta}$ in crack No. α in the direction $\bar{x}_\beta$ is by Ottosen and Dahlblom [27] assumed to be given by

$$\bar{w}^s_{\alpha\beta} = \frac{\bar{w}_\alpha}{G_s}\bar{\sigma}_{\alpha\beta} \quad (\alpha \neq \beta) \tag{2.62}$$

where $\bar{w}_\alpha$ is the crack width, G_s is a material parameter, so-called slip modulus, and $\bar{\sigma}_{\alpha\beta}$ is the shear stress in the crack plane. To obtain a rate formulation Eq. (2.62) is differentiated with respect to time. This yields an expression where the rate of shear displacement is dependent on the rate of the normal stress in addition to the rate of shear stress. This yields, however, a nonsymmetric system of equations. Since it is advantageous to have a symmetric system of equations, the rate of shear displacement and the rate of normal stress may be assumed to be uncoupled. This is obtained by replacing Eq. (2.62) by the relation

$$\dot{\bar{w}}^s_{\alpha\beta} = \frac{\bar{w}_\alpha}{G_s}\dot{\bar{\sigma}}_{\alpha\beta} \tag{2.63}$$

The value of G_s may be expected to increase during development of the elastic modulus E. Thus, the slip modulus may be described as

$$G_s = \eta_E G_{s0} \tag{2.64}$$

where G_{s0} is the slip modulus at time $t_e = t_r$. To get an estimation of G_{s0} one may use the expression

$$G_{s0} = G_{s1}E_0 \tag{2.65}$$

where $G_{s1} = 1.0 \cdot 10^{-4}$ may be chosen on the basis of Paulay and Loeber's data [30].

As in the case of fracture normal to the crack plane, a fracturing strain component is defined for shear displacement. The fracturing shear strain $\bar{\varepsilon}^f_{\alpha\beta}$ is defined by

$$\bar{\varepsilon}^f_{\alpha\beta} = \frac{1}{2}\left(\frac{\bar{w}^s_{\alpha\beta}}{L_\alpha} + \frac{\bar{w}^s_{\beta\alpha}}{L_\beta}\right) \qquad (\alpha \neq \beta) \tag{2.66}$$

where L_α is the equivalent length corresponding to crack No. α as introduced above in Eq. (2.53). Differentiation of Eq. (2.66) with respect to time and substitution of Eqs. (2.53) and (2.63) into the result, and considering that $\dot{\bar{\sigma}}_{\alpha\beta} = \dot{\bar{\sigma}}_{\beta\alpha}$, yields

$$\dot{\bar{\varepsilon}}^f_{\alpha\beta} = A_{\alpha\beta}\dot{\bar{\sigma}}_{\alpha\beta} \qquad (\alpha \neq \beta) \tag{2.67}$$

where

$$A_{\alpha\beta} = \frac{\bar{\varepsilon}^f_{\alpha\alpha} + \bar{\varepsilon}^f_{\beta\beta}}{2G_s} \qquad (\alpha \neq \beta) \tag{2.68}$$

Using Eqs. (2.55) and (2.67) a complete relation between fracturing strain rate and stress rate can be obtained

$$\dot{\bar{\varepsilon}}^f_{pq} = \bar{C}^f_{pqrs}\dot{\bar{\sigma}}_{rs} \tag{2.69}$$

where

$$\bar{C}^f_{1111} = J_1 \tag{2.70}$$

$$\bar{C}^f_{2222} = J_2 \tag{2.71}$$

$$\bar{C}^f_{3333} = J_3 \tag{2.72}$$

$$\bar{C}^f_{1212} = \bar{C}^f_{1221} = \bar{C}^f_{2112} = \bar{C}^f_{2121} = \frac{A_{12}}{2} \tag{2.73}$$

$$\bar{C}^f_{2323} = \bar{C}^f_{2332} = \bar{C}^f_{3223} = \bar{C}^f_{3232} = \frac{A_{23}}{2} \tag{2.74}$$

$$\bar{C}^f_{3131} = \bar{C}^f_{3113} = \bar{C}^f_{1331} = \bar{C}^f_{1313} = \frac{A_{31}}{2} \tag{2.75}$$

All other components $\bar{C}^f_{pqrs}$ are zero.

The stress and fracturing strain rate tensors expressed in the local coordinate system can be transformed to the global coordinate system by the usual relations.

$$\dot{\bar{\sigma}}_{rs} = a_{rk}a_{sm}\dot{\sigma}_{km} \tag{2.76}$$

$$\dot{\varepsilon}^f_{ij} = a_{pi}a_{qj}\dot{\bar{\varepsilon}}^f_{pq} \tag{2.77}$$

where a_{ik} is given by Eq. (2.46), Eqs. (2.69), (2.76) and (2.77) can be combined to form a relation between fracturing strain rate and stress rate in the global coordinate system

$$\dot{\varepsilon}^f_{ij} = a_{pi}a_{qj}\bar{C}^f_{pqrs}a_{rk}a_{sm}\dot{\sigma}_{km} \tag{2.78}$$

2.10 Stress-strain relation

The strain rate tensor $\dot{\varepsilon}$ is assumed to consist of the sum of the strain rates as described in the previous sections, i.e.

$$\dot{\varepsilon}_{ij} = \dot{\varepsilon}^e_{ij} + \dot{\varepsilon}^T_{ij} + \dot{\varepsilon}^{T\sigma}_{ij} + \dot{\varepsilon}^a_{ij} + \dot{\varepsilon}^c_{ij} + \dot{\varepsilon}^f_{ij} \tag{2.79}$$

To obtain a relation between the stress rate $\dot{\sigma}$ and the total strain rate $\dot{\varepsilon}$ the previous expressions will be combined. Substitution of Eqs. (2.15) and (2.78) into Eq. (2.79) yields

$$\dot{\varepsilon}_{ij} = \left(C^e_{ijkm} + a_{pi}a_{qj}\bar{C}^f_{pqrs}a_{rk}a_{sm}\right)\dot{\sigma}_{km} + \dot{\varepsilon}^0_{ij} \tag{2.80}$$

where

$$\dot{\varepsilon}^0_{ij} = \dot{\varepsilon}^T_{ij} + \dot{\varepsilon}^{T\sigma}_{ij} + \dot{\varepsilon}^a_{ij} + \dot{\varepsilon}^c_{ij} \tag{2.81}$$

Since the tensor C^e is isotropic, its components do not change under rotation of the coordinate axes, Eq. (2.80) can be written as

$$\dot{\varepsilon}_{ij} = a_{pi}a_{qj}\bar{C}_{pqrs}a_{rk}a_{sm}\dot{\sigma}_{km} + \dot{\varepsilon}^0_{ij} \tag{2.82}$$

where

$$\bar{C}_{pqrs} = C^e_{pqrs} + \bar{C}^f_{pqrs} \tag{2.83}$$

Eq. (2.82) can be used to determine the strain rate when the stress rate is given. To obtain a finite element formulation, the inverse formulation is of interest.

Therefore, the stiffness tensor $\bar{\mathbf{D}}$ is introduced and defined as the inverse of the compliance tensor $\bar{\mathbf{C}}$, i.e.

$$\bar{D}_{tupq}\bar{C}_{pqrs} = \frac{1}{2}\left(\delta_{tr}\delta_{us} + \delta_{ts}\delta_{ur}\right) \tag{2.84}$$

Multiplication of Eq. (2.82) by $a_{vn}a_{wo}\bar{D}_{vwtu}a_{ti}a_{uj}$, use of the relations $a_{ik}a_{jk} = \delta_{ij}$, $a_{ik}a_{im} = \delta_{km}$, $\dot{\sigma}_{km} = \dot{\sigma}_{mk}$, and Eq. (2.84), and rearrangement yields the relation

$$\dot{\sigma}_{km} = D_{kmij}\dot{\varepsilon}_{ij} - \sigma^0_{km} \tag{2.85}$$

where the material stiffness $\mathbf{D}$ and the pseudo stress rate $\dot{\sigma}^{\mathbf{0}}$ are given by

$$D_{kmij} = a_{rk}a_{sm}\bar{D}_{rspq}a_{pi}a_{qj} \tag{2.86}$$

$$\dot{\sigma}^0_{km} = D_{kmij}\dot{\varepsilon}^0_{ij} \tag{2.87}$$

2.11 Matrix formulation

For computer programming, matrix formulation is in general most convenient. The proposed constitutive equations are therefore summarized below, using matrix notation.

Since the stress and strain tensors are symmetric, the previous equations can be expressed by using six components instead of nine. The constitutive equations, in the present work, are applied to two-dimensional problems, where two of the shear components are zero, and therefore may be excluded. The tensors $\dot{\sigma}$, $\dot{\varepsilon}$ and $\dot{\varepsilon}^{\mathbf{0}}$ are therefore expressed by four-element column matrices, i.e.

$$\dot{\sigma} = \left[\begin{array}{cccc} \dot{\sigma}_{11} & \dot{\sigma}_{22} & \dot{\sigma}_{12} & \dot{\sigma}_{33} \end{array} \right]^T \tag{2.88}$$

$$\dot{\varepsilon} = \left[\begin{array}{cccc} \dot{\varepsilon}_{11} & \dot{\varepsilon}_{22} & 2\dot{\varepsilon}_{12} & \dot{\varepsilon}_{33} \end{array} \right]^T \tag{2.89}$$

$$\dot{\varepsilon}_0 = \left[\begin{array}{cccc} \dot{\varepsilon}^0_{11} & \dot{\varepsilon}^0_{22} & 2\dot{\varepsilon}^0_{12} & \dot{\varepsilon}^0_{33} \end{array} \right]^T \tag{2.90}$$

It should be noted that the shear strain components have been multiplied by 2.

Using matrix notation, Eq. (2.82) can be written

$$\dot{\varepsilon} = \bar{G}\bar{C}\bar{G}^T\dot{\sigma} + \dot{\varepsilon}_0 \tag{2.91}$$

where

$$\bar{G} = \left[\begin{array}{cccc} a_{11}a_{11} & a_{21}a_{21} & a_{11}a_{21} & a_{31}a_{31} \\ a_{12}a_{12} & a_{22}a_{22} & a_{12}a_{22} & a_{32}a_{32} \\ 2a_{11}a_{12} & 2a_{21}a_{22} & a_{11}a_{22} + a_{21}a_{12} & 2a_{31}a_{32} \\ a_{13}a_{13} & a_{23}a_{23} & a_{13}a_{23} & a_{33}a_{33} \end{array} \right] \tag{2.92}$$

$$\bar{C} = \left[\begin{array}{cccc} \frac{1}{E} + J_1 & -\frac{\nu}{E} & 0 & -\frac{\nu}{E} \\ -\frac{\nu}{E} & \frac{1}{E} + J_2 & 0 & -\frac{\nu}{E} \\ 0 & 0 & \frac{2(1+\nu)}{E} + 2A_{12} & 0 \\ -\frac{\nu}{E} & -\frac{\nu}{E} & 0 & \frac{1}{E} + J_3 \end{array} \right] \tag{2.93}$$

$$\dot{\varepsilon}_0 = \dot{\varepsilon}_T + \dot{\varepsilon}_{T\sigma} + \dot{\varepsilon}_c \tag{2.94}$$

$$\dot{\varepsilon}_T = \alpha_T \left(r_T + \beta_T \left(1 - r_T \right) \right) \left[1 \quad 1 \quad 0 \quad 1 \right]^T \tag{2.95}$$

$$\dot{\varepsilon}_{T\sigma} = \beta_{T\sigma} T \left[\begin{array}{cccc} \frac{1}{E_{T\sigma}} & -\frac{\nu_{T\sigma}}{E_{T\sigma}} & 0 & -\frac{\nu_{T\sigma}}{E_{T\sigma}} \\ -\frac{\nu_{T\sigma}}{E_{T\sigma}} & \frac{1}{E_{T\sigma}} & 0 & -\frac{\nu_{T\sigma}}{E_{T\sigma}} \\ 0 & 0 & \frac{2(1+\nu_{T\sigma})}{E_{T\sigma}} & 0 \\ -\frac{\nu_{T\sigma}}{E_{T\sigma}} & -\frac{\nu_{T\sigma}}{E_{T\sigma}} & 0 & \frac{1}{E_{T\sigma}} \end{array} \right] \left[\begin{array}{c} \sigma_{11} \\ \sigma_{22} \\ \sigma_{12} \\ \sigma_{33} \end{array} \right] \tag{2.96}$$

$$\dot{\varepsilon}_c = \sum_{n=1}^{N} \frac{1}{\tau_n} e^{-\frac{t}{\tau_n}} \gamma_n \tag{2.97}$$

$$\gamma_n = \int_0^t e^{\frac{t'}{\tau_n}} \begin{bmatrix} \frac{1}{E_{cn}} & -\frac{\nu_{cn}}{E_{cn}} & 0 & -\frac{\nu_{cn}}{E_{cn}} \\ -\frac{\nu_{cn}}{E_{cn}} & \frac{1}{E_{cn}} & 0 & -\frac{\nu_{cn}}{E_{cn}} \\ 0 & 0 & \frac{2(1+\nu_{cn})}{E_{cn}} & 0 \\ -\frac{\nu_{cn}}{E_{cn}} & -\frac{\nu_{cn}}{E_{cn}} & 0 & \frac{1}{E_{cn}} \end{bmatrix} \begin{bmatrix} \frac{d\sigma_{11}}{dt'} \\ \frac{d\sigma_{22}}{dt'} \\ \frac{d\sigma_{12}}{dt'} \\ \frac{d\sigma_{33}}{dt'} \end{bmatrix} dt' \tag{2.98}$$

Defining G and $\bar{D}$ as

$$G = \bar{G}^{-1} \tag{2.99}$$

$$\bar{D} = \bar{C}^{-1} \tag{2.100}$$

and premultiplying Eq. (2.91) by $G^T DG$ yields

$$\dot{\sigma} = D\dot{\varepsilon} - \dot{\sigma}_0 \tag{2.101}$$

where the material stiffness D and pseudo stress rate $\dot{\sigma}_0$ are given by

$$D = G^T \bar{D} G \tag{2.102}$$

$$\dot{\sigma}_0 = D\dot{\varepsilon}_0 \tag{2.103}$$

For axial symmetry, the matrices given by Eqs. (2.102) and (2.103) can be directly used to establish the element matrices. For plane strain and plane stress, the matrices have to be reduced to three components, using the conditions $\dot{\varepsilon}_{33} = 0$ and $\dot{\sigma}_{33} = 0$, respectively, before establishing element matrices.

Chapter 3

DESCRIPTION OF THEORY FOR COMPUTATION OF TEMPERATURE

3.1 Introduction

To facilitate simulation of thermal problems numerical methods are used. The finite element method has proved to be an efficient tool in thermal analysis and is therefore applied. In this chapter a finite element formulation of the heat conduction problem is given. An infinite element formulation is also given. This concept is applied to take into account unbounded regions of e.g. rock.

3.2 Finite element formulation

In order to arrive at an appropriate finite element formulation, the basic equations of heat conduction will be briefly described.

The heat balance equation is given by

$$\frac{\partial q_i}{\partial x_i} + \rho c \dot{T} - Q = 0 \tag{3.1}$$

where $\mathbf{q}$ is the heat flow vector, ρ is the mass density, c is the specific heat, T is the temperature, Q is the generated heat according to Eq. (2.9) and x_i denotes a Cartesian coordinate system. Eq. (3.1) is multiplied by a set of weighting functions v_m and an integration over the studied body volume V is performed

$$\int_V v_m \frac{\partial q_i}{\partial x_i} dV + \int_V v_m \rho c \dot{T} dV - \int_V v_m Q dV = 0 \tag{3.2}$$

It should be noted that the index m may normally assume values exceeding 3.

Use of the divergence theorem gives the relation

$$-\int_V \frac{\partial v_m}{\partial x_i} q_i dV + \int_V v_m \rho c \dot{T} dV = \int_S v_m q_s dS + \int_V v_m Q dV \tag{3.3}$$

where q_s is the heat flow into the body studied, given by

$$q_s = -q_i n_i \tag{3.4}$$

where $\mathbf{n}$ is the outward unit vector normal to the surface S.

The heat flow is related to the temperature gradient by the Fourier law for thermal conduction, i.e.

$$q_i = -k \frac{\partial T}{\partial x_i} \tag{3.5}$$

where k is the thermal conductivity.

Substitution of Eq. (3.5) into Eq. (3.3) yields

$$\int_V \frac{\partial v_m}{\partial x_i} k \frac{\partial T}{\partial x_i} dV + \int_V v_m \rho c \dot{T} dV = \int_S v_m q_s dS + \int_V v_m Q dV \tag{3.6}$$

In order to obtain finite element equations the temperature T is expressed as a function of the nodal temperatures $\bar{T}_n$ as

$$T = N_n \bar{T}_n \tag{3.7}$$

where N_n are interpolation functions. The summation index n in Eq. (3.7) may normally exceed 3.

According to the Galerkin method the interpolation functions are chosen as weighting functions, i.e.

$$v_m = N_m \tag{3.8}$$

Substitution of Eqs. (3.7) and (3.8) into Eq. (3.6) yields

$$K_{mn} \bar{T}_n + C_{mn} \dot{\bar{T}}_n = P_m \tag{3.9}$$

where

$$K_{mn} = \int_V \frac{\partial N_m}{\partial x_i} k \frac{\partial N_n}{\partial x_i} dV \tag{3.10}$$

$$C_{mn} = \int_V N_m \rho c N_n dV \tag{3.11}$$

$$P_m = \int_S N_m q_s dS + \int_V N_m Q dV \tag{3.12}$$

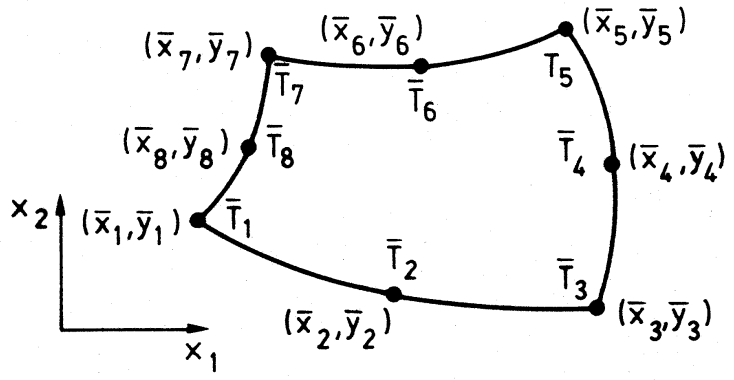

Figure 3.1: Geometry and degrees of freedom of eight-node isoparametric element

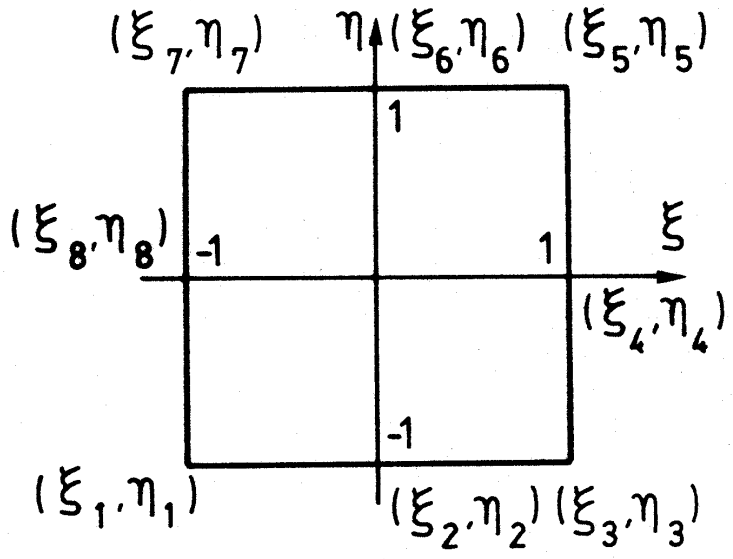

Figure 3.2: Parent element

The present work deals with plane and axisymmetric problems, using an eight-node isoparametric element, see Fig. 3.1. The element is obtained by distorting the rectangular parent element of Fig. 3.2.

The geometry of the element is given by the relations

$$x_1 = N_n \bar{x}_n \tag{3.13}$$

and

$$x_2 = N_n \bar{y}_n \tag{3.14}$$

where the interpolation functions, N_n may be found in e.g. Zienkiewicz and Taylor [37] and are given by

$$\begin{array}{ll} N_1 = \frac{1}{4}(1-\xi)(1-\eta)(-\xi-\eta-1); & N_2 = \frac{1}{2}(1-\xi^2)(1-\eta); \\ N_3 = \frac{1}{4}(1+\xi)(1-\eta)(\xi-\eta-1); & N_4 = \frac{1}{2}(1+\xi)(1-\eta^2); \\ N_5 = \frac{1}{4}(1+\xi)(1+\eta)(\xi+\eta-1); & N_6 = \frac{1}{2}(1-\xi^2)(1+\eta); \\ N_7 = \frac{1}{4}(1-\xi)(1+\eta)(-\xi+\eta-1); & N_8 = \frac{1}{2}(1-\xi)(1-\eta^2) \end{array} \tag{3.15}$$

The interpolation functions N_n of Eq. (3.15) are used also for the temperature in Eq. (3.7).

According to the chain rule, the derivatives of N_n with respect to ξ and η can be expressed in the derivatives with respect to x_1 and x_2 as

$$\begin{bmatrix} \frac{\partial N_n}{\partial \xi} \\ \frac{\partial N_n}{\partial \eta} \end{bmatrix} = J \begin{bmatrix} \frac{\partial N_n}{\partial x_1} \\ \frac{\partial N_n}{\partial x_2} \end{bmatrix} \tag{3.16}$$

where J is the Jacobian matrix given by

$$J = \begin{bmatrix} \frac{\partial x_1}{\partial \xi} & \frac{\partial x_2}{\partial \xi} \\ \frac{\partial x_1}{\partial \eta} & \frac{\partial x_2}{\partial \eta} \end{bmatrix} \tag{3.17}$$

Substitution of Eqs. (3.13) and (3.14) into Eq. (3.17) yields

$$J = \begin{bmatrix} \frac{\partial N_n}{\partial \xi}\bar{x}_n & \frac{\partial N_n}{\partial \xi}\bar{y}_n \\ \frac{\partial N_n}{\partial \eta}\bar{x}_n & \frac{\partial N_n}{\partial \eta}\bar{y}_n \end{bmatrix} \tag{3.18}$$

The derivatives of N_n with respect to x_1 and x_2 can be obtained from Eq. (3.16), i.e.

$$\begin{bmatrix} \frac{\partial N_n}{\partial x_1} \\ \frac{\partial N_n}{\partial x_2} \end{bmatrix} = J^{-1} \begin{bmatrix} \frac{\partial N_n}{\partial \xi} \\ \frac{\partial N_n}{\partial \eta} \end{bmatrix} \tag{3.19}$$

where J^{-1} is the inverse of the Jacobian matrix J of Eq. (3.18). The derivatives of N_n with respect to ξ and η are obtained by differentiation of the expressions of Eq.

(3.15), i.e.

$$\begin{array}{ll}
\frac{\partial N_1}{\partial \xi} = \frac{1}{4}(1-\eta)(2\xi+\eta); & \frac{\partial N_2}{\partial \xi} = -\xi(1-\eta); \\
\frac{\partial N_3}{\partial \xi} = \frac{1}{4}(1-\eta)(2\xi-\eta); & \frac{\partial N_4}{\partial \xi} = \frac{1}{2}(1-\eta^2); \\
\frac{\partial N_5}{\partial \xi} = \frac{1}{4}(1+\eta)(2\xi+\eta); & \frac{\partial N_6}{\partial \xi} = -\xi(1+\eta); \\
\frac{\partial N_7}{\partial \xi} = \frac{1}{4}(1+\eta)(2\xi-\eta); & \frac{\partial N_8}{\partial \xi} = -\frac{1}{2}(1-\eta^2); \\
\frac{\partial N_1}{\partial \eta} = \frac{1}{4}(1-\xi)(2\eta+\xi); & \frac{\partial N_2}{\partial \eta} = -\frac{1}{2}(1-\xi^2); \\
\frac{\partial N_3}{\partial \eta} = \frac{1}{4}(1+\xi)(2\eta-\xi); & \frac{\partial N_4}{\partial \eta} = -\eta(1+\xi); \\
\frac{\partial N_5}{\partial \eta} = \frac{1}{4}(1+\xi)(2\eta+\xi); & \frac{\partial N_6}{\partial \eta} = \frac{1}{2}(1-\xi^2); \\
\frac{\partial N_7}{\partial \eta} = \frac{1}{4}(1-\xi)(2\eta-\xi); & \frac{\partial N_8}{\partial \eta} = -\eta(1-\xi)
\end{array} \tag{3.20}$$

The volume integrals of Eqs. (3.10)-(3.12) are transformed into integrals over the area of the parent element by the substitution

$$dV = t\det(J)d\xi d\eta \tag{3.21}$$

for plane problems and

$$dV = 2\pi x_1 \det(J)d\xi d\eta \tag{3.22}$$

for axisymmetric problems, with x_1 and x_2 as radial and axial coordinate, respectively. The integrals can be evaluated numerically by Gauss quadrature as

$$\int_{-1}^{1}\int_{-1}^{1} f(\xi,\eta)\,d\xi d\eta = \sum_{j=1}^{n}\sum_{i=1}^{n} H_i H_j f(\xi_i,\eta_j) \tag{3.23}$$

where, for $n = 2$,

$$H_1 = H_2 = 1 \tag{3.24}$$

$$\xi_1 = \eta_1 = -\frac{1}{\sqrt{3}} \tag{3.25}$$

$$\xi_2 = \eta_2 = \frac{1}{\sqrt{3}} \tag{3.26}$$

For other values of n the H_i, ξ_i and η_i values may be found in e.g. Zienkiewicz and Taylor [37].

The surface integral of Eq. (3.12) is transformed into an integral over the side of a parent element by the substitution

$$dS = t\sqrt{\left[\frac{dx}{d\xi}\right]^2 + \left[\frac{dy}{d\xi}\right]^2}\,d\xi \tag{3.27}$$

for plane problems and

$$dS = 2\pi x_1\sqrt{\left[\frac{dx}{d\xi}\right]^2 + \left[\frac{dy}{d\xi}\right]^2}\,d\xi \tag{3.28}$$

for axisymmetric problems.

The integral can be evaluated numerically by Gauss quadrature as

$$\int_{-1}^{1} f(\xi)d\xi = \sum_{i=1}^{n} H_i f(\xi_i) \tag{3.29}$$

A prescribed heat flow into the body studied is represented by the quantity q_s in Eq. (3.12). To consider the influence of a prescribed environmental temperature, the heat flow q_s is assumed to be given by the relation

$$q_s = \alpha_t \left(T_0 - T\right) \tag{3.30}$$

where α_t is the transfer coefficient, T_0 is the environmental temperature and T is the surface temperature.

Substitution of Eq. (3.7) into Eq. (3.30) yields

$$q_s = \alpha_t T_0 - \alpha_t N_n \bar{T}_n \tag{3.31}$$

Since the second term of Eq. (3.31) is a function of the nodal temperatures $\bar{T}_n$, the integral of this term should be moved to the left-hand side of Eq. (3.9).

3.3 Infinite element formulation

Casting of concrete is often performed with an unbounded region of e.g. rock as neighbouring material. A simple method of considering the heat exchange between the concrete and the unbounded neighbouring material, is to include the unbounded region in the finite element mesh and truncate the mesh at some great, but finite, distance. This method is, however, expensive and sometimes inaccurate, owing to difficulties in positioning the finite boundary. A successful method of dealing with unbounded regions is to couple mapped infinite elements, see Refs. [36], [12], [25], to the finite element mesh.

In the present work, an infinite element is used, which may be regarded as a modification of the eight-node isoparametric element described above. This means that the interpolation functions N_n of Eq. (3.15) are still used for the temperature, but for the geometry the functions N_n are replaced by mapping functions which make the element extend to infinity. Two versions of infinite elements are used; namely singly infinite elements, which extend to infinity in the η-direction, and doubly infinite elements, which extend to infinity in both the ξ-direction and the η-direction. The singly infinite element has five finite nodes, as shown in Fig. 3.3.

The mapping functions to be used instead of Eq. (3.15) in Eqs. (3.13) and (3.14) are, according to Marques and Owen [25], given by

$$\begin{aligned} N_1 &= \tfrac{(1-\xi)(-\xi-\eta-1)}{1-\eta}; & N_2 &= \tfrac{2\left(1-\xi^2\right)}{1-\eta}; \\ N_3 &= \tfrac{(1+\xi)(\xi-\eta-1)}{1-\eta}; & N_4 &= \tfrac{(1+\xi)(1+\eta)}{2(1-\eta)}; \\ & & N_8 &= \tfrac{(1-\xi)(1+\eta)}{2(1-\eta)} \end{aligned} \tag{3.32}$$

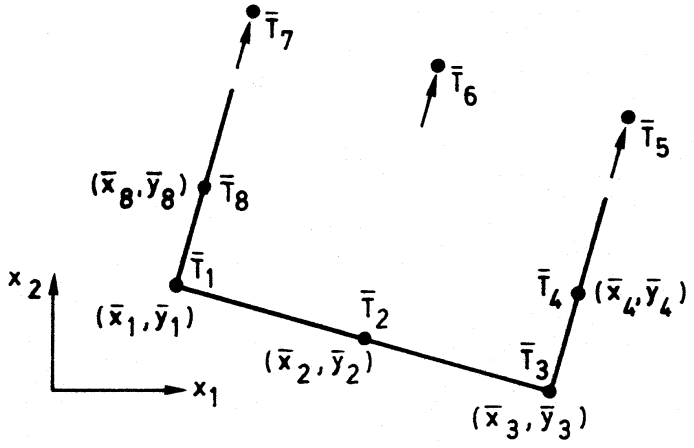

Figure 3.3: Geometry and degrees of freedom of five-node singly infinite element

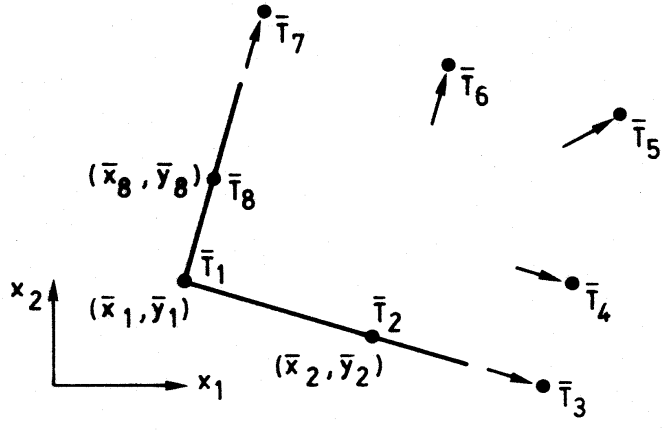

Figure 3.4: Geometry and degrees of freedom of three-node doubly infinite element

Differentation of the expressions in Eq. (3.20) yields

$$\begin{array}{ll} \frac{\partial N_1}{\partial \xi} = \frac{2\xi+\eta}{1-\eta}; & \frac{\partial N_2}{\partial \xi} = -\frac{4\xi}{1-\eta}; \\ \frac{\partial N_3}{\partial \xi} = \frac{2\xi-\eta}{1-\eta}; & \frac{\partial N_4}{\partial \xi} = \frac{1+\eta}{2(1-\eta)}; \\ & \frac{\partial N_8}{\partial \xi} = -\frac{1+\eta}{2(1-\eta)}; \\ \frac{\partial N_1}{\partial \eta} = \frac{-2+\xi+\xi^2}{(1-\eta)^2}; & \frac{\partial N_2}{\partial \eta} = \frac{2(1-\xi^2)}{(1-\eta)^2}; \\ \frac{\partial N_3}{\partial \eta} = \frac{-2-\xi+\xi^2}{(1-\eta)^2}; & \frac{\partial N_4}{\partial \eta} = \frac{1+\xi}{(1-\eta)^2}; \\ & \frac{\partial N_8}{\partial \eta} = \frac{1-\xi}{(1-\eta)^2} \end{array} \tag{3.33}$$

which should be used in Eq. (3.18) instead of the expressions in Eq. (3.20).

The doubly infinite element has three finite nodes, as shown in Fig. 3.4.

The mapping functions to be used instead of Eq. (3.15) in Eqs. (3.13) and (3.14) are, according to Marques and Owen [25], given by

$$\begin{array}{ll} N_1 = \frac{\xi\eta+3(-\xi-\eta-1)}{(1-\xi)(1-\eta)}; & N_2 = \frac{2(1+\xi)}{(1-\xi)(1-\eta)}; \\ & N_8 = \frac{2(1+\eta)}{(1-\xi)(1-\eta)} \end{array} \tag{3.34}$$

Differentation of Eqs. (3.34) yields

$$\begin{array}{ll} \frac{\partial N_1}{\partial \xi} = -\frac{2(3+\eta)}{(1-\xi)^2(1-\eta)}; & \frac{\partial N_2}{\partial \xi} = \frac{4}{(1-\xi)^2(1-\eta)}; \\ & \frac{\partial N_8}{\partial \xi} = \frac{2(1+\eta)}{(1-\xi)^2(1-\eta)}; \\ \frac{\partial N_1}{\partial \eta} = -\frac{2(3+\xi)}{(1-\xi)(1-\eta)^2}; & \frac{\partial N_2}{\partial \eta} = \frac{2(1+\xi)}{(1-\xi)(1-\eta)^2}; \\ & \frac{\partial N_8}{\partial \eta} = \frac{4}{(1-\xi)(1-\eta)^2} \end{array} \tag{3.35}$$

which should be used in Eq. (3.18) instead of the expressions in Eq. (3.20).

The nodes at infinity are assumed to have a constant temperature. Therefore, the terms $K_{mn}\bar{T}_n$ in Eq. (3.9) which correspond to nodes at infinity are known and can be moved to the right-hand side. Since the temperature at the infinite nodes is constant, the time derivatives are zero. This means that a set of equations, expressed in the finite nodes only, is obtained.

3.4 Numerical solution procedure

In Section 3.2 finite element equations have been established, cf. Eq. (3.9). To determine the nodal temperatures $\bar{T}_n$ at time t, these equations are integrated with respect to time using a recurrence relation, see e.g. Zienkiewicz and Taylor [38]. A recurrence relation obtained from Eq. (3.9) can be written as

$$\left[\theta K_{mn} + \frac{1}{\Delta t} C_{mn}\right] \bar{T}_n(t) = P_m - \left[(1-\theta) K_{mn} - \frac{1}{\Delta t} C_{mn}\right] \bar{T}_n(t-\Delta t) \tag{3.36}$$

where Δt is the time step, $\bar{T}_n(t)$ is the nodal temperature at time t, and $\bar{T}_n(t-\Delta t)$ is the nodal temperature at time $t-\Delta t$, which is assumed to be known. The

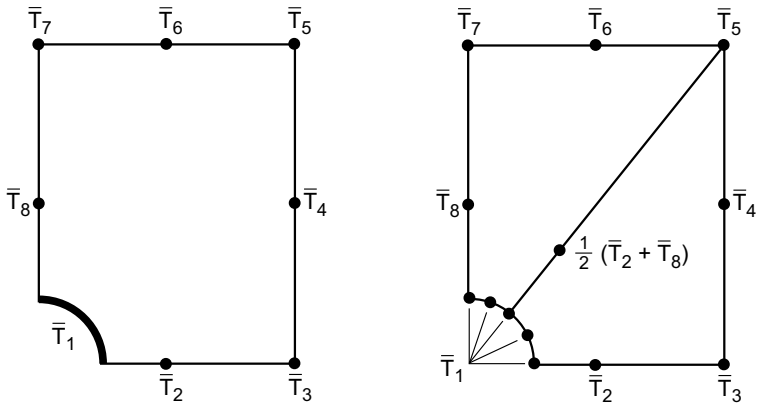

Figure 3.5: Geometry and degrees of freedom for element for pipe modelling

parameter θ is in the present work chosen as $\theta = 1$. With this choice Eq. (3.31) can be written as

$$\bar{K}_{mn}\bar{T}_n\left(t\right) = \bar{P}_m \tag{3.37}$$

where

$$\bar{K}_{mn} = K_{mn} + \frac{1}{\Delta t}C_{mn} \tag{3.38}$$

$$\bar{P}_m = P_m + \frac{1}{\Delta t}C_{mn}\bar{T}_n\left(t - \Delta t\right) \tag{3.39}$$

This procedure is known as a backward difference method and is unconditionally stable.

3.5 Cooling pipes

In order to prevent the temperature from increasing too much during the hardening process cooling pipes may be cast into the concrete. One way to consider cooling pipes in the analysis is to simply prescribe the temperature at the nodes where the pipes are positioned. When the diameter of the cooling pipes is considerable this procedure may be inaccurate. In the present program it is possible to model the influence from cooling pipes in an alternative manner. To consider the influence from the pipe dimension a special purpose element is used for modelling of the concrete neighbouring a pipe, see Fig. 3.5. This element is obtained by combining two eight-node elements and assuming the five nodes at the pipe surface to have the same temperature. The mid-side node connecting the two elements is positioned at a distance from the pipe centre corresponding to the average distance to the pipe centre for the nodes 2 and 8 in the figure and is eliminated assuming the temperature to be the average of the temperatures of these nodes. In this manner an element is obtained which can be handled as the ordinary elements but considers the pipe dimension.

In addition to pipe diameter, the transfer coefficient of the pipe wall and the temperature inside the pipe are used in the computation. For determination of the pipe temperature it is considered that a pipe arrangement may consist of several pipe parts connected to each other. Each pipe part is assumed to have the length l_p perpendicular to the plane of computation. To each arrangement the input temperature T_{in} and either output temperature T_{out} or pipe flow q_p has to be specified. An approximative value of the heat Q_p to be removed from the concrete by the pipe arrangement can be obtained from the results of the previous time step as

$$Q_p = \sum_{i_p=1}^{n_p} q_{i_p} l_p \tag{3.40}$$

where q_{i_p} is the heat transport from pipe part i_p.

If output temperature has been specified, the flow q_p required in the pipe arrangement can be determined by

$$q_p = \frac{Q_p}{c_w(T_{out} - T_{in})} \tag{3.41}$$

where c_w is the specific heat of the cooling medium, for water $c_w = 4.2kJ/kgK$. If instead the pipe flow has been specified the output temperature is given by

$$T_{out} = T_{in} + \frac{Q_p}{c_w q_p} \tag{3.42}$$

The temperature to be prescribed in the node corresponding the first pipe part can be assumed to be the input temperature T_{in} plus the temperature increase obtained in the first half of the pipe part, i.e.

$$T_1 = T_{in} + \frac{Q_1}{c_w q_p} \tag{3.43}$$

where

$$Q_1 = \frac{q_1 l_p}{2} \tag{3.44}$$

is the heat removed from the concrete by one half of the pipe part. The temperature to be prescribed in a following node i can then be determined by

$$T_i = T_{i-1} + \frac{(Q_{i-1} + Q_i)}{c_w q_p} \tag{3.45}$$

Chapter 4

DESCRIPTION OF THEORY FOR COMPUTATION OF DISPLACEMENTS AND STRESSES

4.1 Introduction

In the previous chapter the theory for computation of temperatures was described. The temperature distributions obtained are used as input for the computation of displacements and stresses. The theory for this computation will be described in this chapter. Just as for computation of temperatures, the finite element method is used for computation of displacements and stresses. This chapter presents a finite element formulation of the displacement and stress problem.

4.2 Finite element formulation

The basic equations of nonlinear structural analysis will be briefly described and a finite element formulation will be established.

The equations of equilibrium are

$$\frac{\partial \sigma_{ij}}{\partial x_j} + f_j = 0 \tag{4.1}$$

where σ is the stress tensor, f is the vector representing body force per unit volume and x_j denotes a Cartesian coordinate system. Eq. (4.1) is multiplied by a set of weighting functions v_{im} and an integration is performed over the studied volume V, which yields

$$\int_V v_{im} \frac{\partial \sigma_{ji}}{\partial x_j} dV + \int_V v_{im} f_i dV = 0 \tag{4.2}$$

The index m may normally exceed 3. Using the divergence theorem yields

$$\int_V \frac{\partial v_{im}}{\partial x_j}\sigma_{ji}dV = \int_S v_{im}t_i dS + \int_V v_{im}f_i dV \tag{4.3}$$

where t is the traction vector defined by

$$t_i = \sigma_{ji}n_j \tag{4.4}$$

where n is the outward unit vector normal to the surface S of the body studied. Since v_{im} is assumed to be constant with respect to time, Eq. (4.3) yields

$$\int_V \frac{\partial v_{im}}{\partial x_j}\dot{\sigma}_{ji}dV = \int_S v_{im}\dot{t}_i dS + \int_V v_{im}\dot{f}_i dV \tag{4.5}$$

In Chapter 2 the relation between stress rate $\dot{\sigma}$ and strain rate $\dot{\varepsilon}$ was expressed as (cf. Eq. 2.85)

$$\dot{\sigma}_{ij} = D_{jipq}\dot{\varepsilon}_{pq} - \dot{\sigma}^0_{ji} \tag{4.6}$$

where $\mathbf{D}$ is the material stiffness and $\dot{\sigma}^0$ is the rate of pseudo stress. The strain rate $\dot{\varepsilon}$ is assumed to be given by the kinematic relation

$$\dot{\varepsilon}_{pq} = \frac{1}{2}\left[\frac{\partial u_p}{\partial x_q} + \frac{\partial u_q}{\partial x_p}\right] \tag{4.7}$$

where $\mathbf{u}$ is the displacement vector.

Eqs. (4.5), (4.6) and (4.7) are combined to form the relation

$$\int_V \frac{\partial v_{im}}{\partial x_j}D_{jipq}\frac{1}{2}\left[\frac{\partial \dot{u}_p}{\partial x_q} + \frac{\partial \dot{u}_q}{\partial x_p}\right]dV = \int_S v_{im}\dot{t}_i dS + \int_V v_{im}\dot{f}_i dV + \int_V \frac{\partial v_{im}}{\partial x_j}\dot{\sigma}^0_{ji}dV \tag{4.8}$$

Since the stress rate and strain rate tensors $\dot{\sigma}$ and $\dot{\varepsilon}$ are symmetric, the material stiffness tensor $\mathbf{D}$ has the symmetry properties

$$D_{ijpq} = D_{jipq} \tag{4.9}$$

$$D_{ijpq} = D_{ijqp} \tag{4.10}$$

Due to these symmetry properties, Eq. (4.8) can be written as

$$\int_V \frac{\partial v_{im}}{\partial x_j}D_{ijpq}\frac{\partial \dot{u}_p}{\partial x_q}dV = \int_S v_{im}\dot{t}_i dS + \int_V v_{im}\dot{f}_i dV + \int_V \frac{\partial v_{im}}{\partial x_j}\dot{\sigma}^0_{ji}dV \tag{4.11}$$

To obtain finite element equations, the displacements u are expressed as a function of the nodal displacements $\bar{u}_n$ as

$$u_p = \bar{N}_{pn}\bar{u}_n \tag{4.12}$$

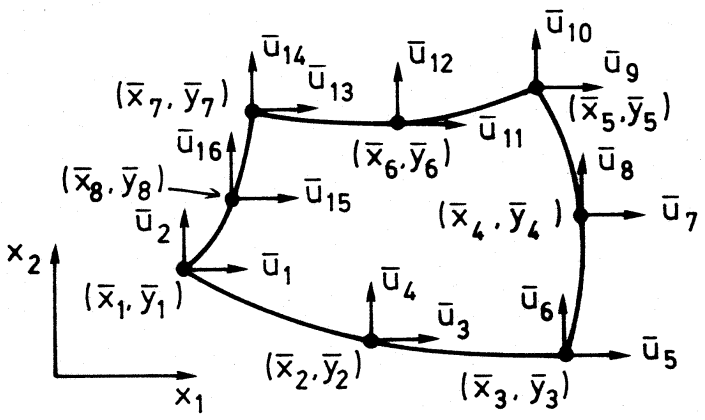

Figure 4.1: Geometry and degrees of freedom of eight-node isoparametric element

where $\bar{N}_{pm}$ are interpolation functions. The summation index in Eq. (4.12) may normally exceed 3. Since the interpolation functions $\bar{N}_{pn}$ are assumed to be constant with respect to time, differentiation of Eq. (4.12) yields

$$\dot{u}_p = \bar{N}_{pn}\dot{\bar{u}}_n \tag{4.13}$$

The interpolation functions are chosen as weighting functions, according to the Galerkin method, i.e.

$$v_{im} = \bar{N}_{im} \tag{4.14}$$

Substitution of Eqs. (4.13) and (4.14) into Eq. (4.11) yields

$$K_{mn}\dot{\bar{u}}_n = \dot{P}_m + \dot{P}^0_m \tag{4.15}$$

where

$$K_{mn} = \int_V \frac{\partial \bar{N}_{im}}{\partial x_j} D_{ijpq} \frac{\partial \bar{N}_{pn}}{\partial x_q} dV \tag{4.16}$$

$$\dot{P}_m = \int_S \bar{N}_{im}\dot{t}_i dS + \int_V \bar{N}_{im}\dot{f}_i dV \tag{4.17}$$

$$\dot{P}^0_m = \int_V \frac{\partial \bar{N}_{im}}{\partial x_j}\dot{\sigma}^0_{ij} dV \tag{4.18}$$

The present work deals with plane stress, plane strain and axisymmetric problems and, just as for temperatures described in Chapter 3, an eight-node isoparametric element is used, see Fig. 4.1.

The element is obtained by distorting the rectangular parent element shown in Fig. 4.2. The geometry of the element is given by the relations

$$x_1 = N_n \bar{x}_n \tag{4.19}$$

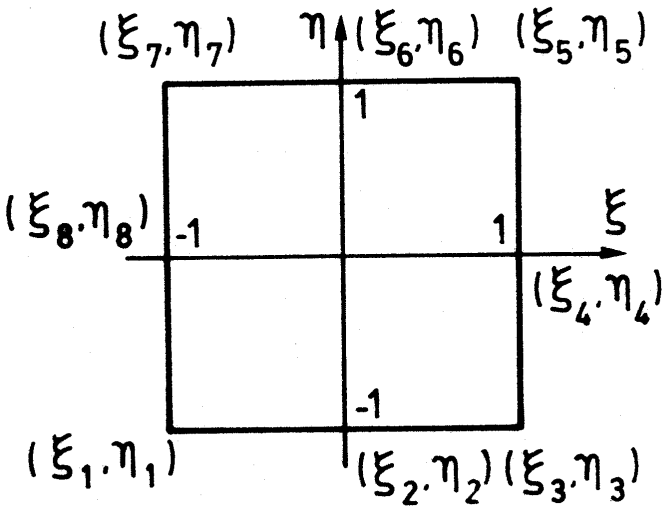

Figure 4.2: Parent element

and

$$x_2 = N_n \bar{y}_n \tag{4.20}$$

where the interpolation functions N_n are given by Eq. (3.15).

The interpolation functions $\bar{N}_{pn}$ for displacements, introduced in Eq. (4.12), are given by the relations

$$\begin{aligned} \bar{N}_{1\ 2n-1} &= N_n; \quad N_{1\ 2n} = 0; \\ \bar{N}_{2\ 2n-1} &= 0; \quad\ \ N_{2\ 2n} = N_n \end{aligned} \tag{4.21}$$

To obtain a formulation suitable for computer programming, the symmetry properties of the tensors $\mathbf{D}$ and $\dot{\sigma}^0$, and the fact that some terms are zero for plane and axisymmetric problems, can be utilized. Eqs. (4.16) - (4.18) can thus be expressed as

$$K_{mn} = \int_V B_m^T D B_n dV \tag{4.22}$$

$$\dot{P}_m = \int_S N_m^T t dS + \int_V N_m^T f dV \tag{4.23}$$

$$\dot{P}_m^0 = \int_V B_m^T \dot{\sigma}^0 dV \tag{4.24}$$

where D and $\dot{\sigma}^0$ are defined by Eqs. (2.102) and (2.103) and the matrices $\dot{t}$, $\dot{f}$, and N_n^T are given by

$$\dot{t} = \begin{bmatrix} \dot{t}_1 & \dot{t}_2 \end{bmatrix}^T \tag{4.25}$$

$$f = \begin{bmatrix} f_1 & f_2 \end{bmatrix}^T \tag{4.26}$$

$$\bar{N}_n = \begin{bmatrix} \bar{N}_{1\ n} & \bar{N}_{2\ n} \end{bmatrix}^T \tag{4.27}$$

The matrix B_n is for plane stress and plane strain given by

$$B_n = \begin{bmatrix} \frac{\partial \bar{N}_{1\ n}}{\partial x_1} & \frac{\partial \bar{N}_{2\ n}}{\partial x_2} & \frac{\partial \bar{N}_{1\ n}}{\partial x_2} + \frac{\partial \bar{N}_{2\ n}}{\partial x_1} \end{bmatrix}^T \tag{4.28}$$

and for axisymmetric analysis defined as

$$B_n = \begin{bmatrix} \frac{\partial \bar{N}_{1\ n}}{\partial x_1} & \frac{\partial \bar{N}_{2\ n}}{\partial x_2} & \frac{\partial \bar{N}_{1\ n}}{\partial x_2} + \frac{\partial \bar{N}_{2\ n}}{\partial x_1} & \frac{\bar{N}_{1\ n}}{x_1} \end{bmatrix}^T \tag{4.29}$$

The derivatives of the shape functions are given by Eq. (3.19) and the integrals in Eqs. (4.22) - (4.24) are evaluated by Gauss quadrature according to Eqs. (3.23) and (3.29).

4.3 Numerical solution procedure

To determine the nodal displacements $\bar{u}_n$ at time t, Eq. (4.15) is integrated with respect to time, using a numerical procedure. The numerical solution procedure includes approximations, which may result in that the equations of equilibrium are not satisfied exactly. The so-called out-of-balance forces P_m^* are defined as the difference between the right and left-hand sides of Eq. (4.3), i.e.

$$P_m^* = \int_S v_{im} t_i dS + \int_V v_{im} f_i dV - \int_V \frac{\partial V_{im}}{\partial x_j} \sigma_{ji} dV \tag{4.30}$$

The matrices t and f, defined by

$$t = \begin{bmatrix} t_1 & t_2 \end{bmatrix}^T \tag{4.31}$$

$$f = \begin{bmatrix} f_1 & f_2 \end{bmatrix}^T \tag{4.32}$$

and σ, which for plane stress and plane strain is given by

$$\sigma = \begin{bmatrix} \sigma_{11} & \sigma_{22} & \sigma_{12} \end{bmatrix}^T \tag{4.33}$$

and for axial symmetri given by

$$\sigma = \begin{bmatrix} \sigma_{11} & \sigma_{22} & \sigma_{12} & \sigma_{33} \end{bmatrix}^T \tag{4.34}$$

and Eqs. (4.14), (4.27) and (4.28) or (4.29) can be combined with Eq. (4.30) to form the expression

$$P_m^* = P_m - \int_V B_m^T \sigma dV \tag{4.35}$$

where the total external loads P_m are given by

$$P_m = \int_S N_m^T t dS + \int_V N_m^T f dV \tag{4.36}$$

The last term in Eq. (4.35) represents the internal forces, corresponding to the stress obtained σ, as computed according to the constitutive equations. Differentiation of Eq. (4.35) with respect to time yields the rate of change of the out-of-balances forces P_m^*, i.e.

$$\dot{P}_m^* = \dot{P}_m - \int_V B_m^T \dot{\sigma} dV \tag{4.37}$$

Substitution of Eq. (2.101) and the relation

$$\dot{\varepsilon} = B_n \dot{\bar{u}}_n \tag{4.38}$$

into Eq. (4.37) yields the expression

$$K_{mn} \dot{\bar{u}}_n = \dot{P}_m + \dot{P}_m^0 - \dot{P}_m^* \tag{4.39}$$

where K_{mn} and $\dot{P}_m^0$ are defined by Eqs. (4.22) and (4.23), respectively.

Evaluation of Eq. (4.39) can be performed by an Euler forward expression, assuming a linear relation from time t to time $t + \Delta t$, i.e.

$$K_{mn}(t) \Delta \bar{u}_n = \Delta P_m + \Delta t \dot{P}_m^0(t) - \Delta t \dot{P}_m^* \tag{4.40}$$

where $K_{mn}(t)$ is the tangential stiffness at time t, $\Delta \bar{u}_n$ the change of nodal displacements from time t to time $t + \Delta t$, $\dot{P}_m^0(t)$ the rate of pseudo load at time t, and ΔP_m incremental load, given by

$$\Delta P_m = \int_t^{t+\Delta t} \dot{P}_m dt \tag{4.41}$$

The rate of change of the out-of-balance forces $\dot{P}_m^*$ is assumed to be given by

$$\dot{P}_m^* = -\frac{1}{\Delta t} P_m^*(t) \tag{4.42}$$

to make the out-of-balance forces reduce to zero, during the time increment, and guide the solution towards the true one. Substitution of Eq. (4.42) into Eq. (4.40) yeilds

$$K_{mn}(t) \Delta \bar{u}_n = \Delta P_m + \Delta t \dot{P}_m^0(t) + P_m^*(t) \tag{4.43}$$

This procedure is described by Stricklin et al. [33], and is called a self-correcting form, since the solution is guided towards the true one. Making $\dot{P}_m^* = 0$ in Eq. (4.40) yields a purely incremental stiffness method, which yields solutions with a tendency to drift away from the true solution, because of increasing out-of-balance forces.

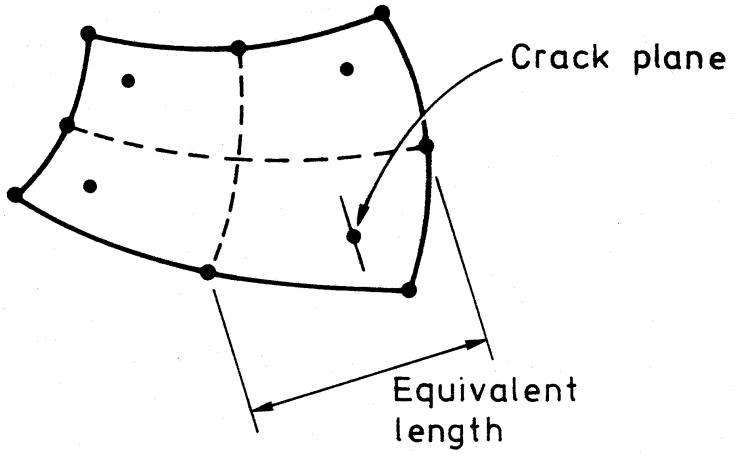

Figure 4.3: Illustration of equivalent length in eight-node element with four integration points.

4.4 Definition of equivalent length

In Eqs. (2.54) and (2.66), when the fracturing strain was defined, an equivalent length L_α was introduced. This length is related to the size of the finite element where the crack develops. In the present work the equivalent length is chosen according to the definition proposed by Ottosen and Dahlblom [27]. The equivalent length is thus defined as the maximum length of the element region of interest, in the direction normal to the crack plane. For an eight-node element, the region bounded by the nodal points closest to the integration point in question and the element mid-point is considered. This definition is illustrated in Fig. 4.3.

Chapter 5

COMPUTER PROGRAM

5.1 General remarks

In this chapter a brief description of the computer program, which is based on the theory presented in Chapters 2, 3 and 4 will be given.

The program can be used for simulation of the temperature and stress in two dimensional and axisymmetric concrete structures during hardening. When computation of stress is performed it is possible to choose whether to compute temperature and maturity or not. If maturity and temperature are not to be computed, it is possible to provide these data as input to a stress computation. The computer program includes an algorithm for providing such an input file on the basis of determination of mean values of temperature and maturity obtained from a simulation in a plane perpendicular to the one where stresses are to be simulated. The program also includes code for determination of heat development parameters, according to the description in Appendix B.

The program has a graphical user interface, see Fig. 5.1. To define the computational model the program user specifies geometry, material properties, and boundary conditions. On the basis of the data specified a finite element mesh is generated. When the computation has been performed, output data can be presented graphically and numerically. The program includes facilities for transfer of output data to e.g. word processing programs or spreadsheet programs, to facilitate further data processing or report production.

The manner of generation of input data and presentation of output data are described in the following sections.

5.2 Generation of input data

As input data the program user specifies geometry, material properties, and boundary conditions. Based on the specified data, the program generates a finite element mesh.

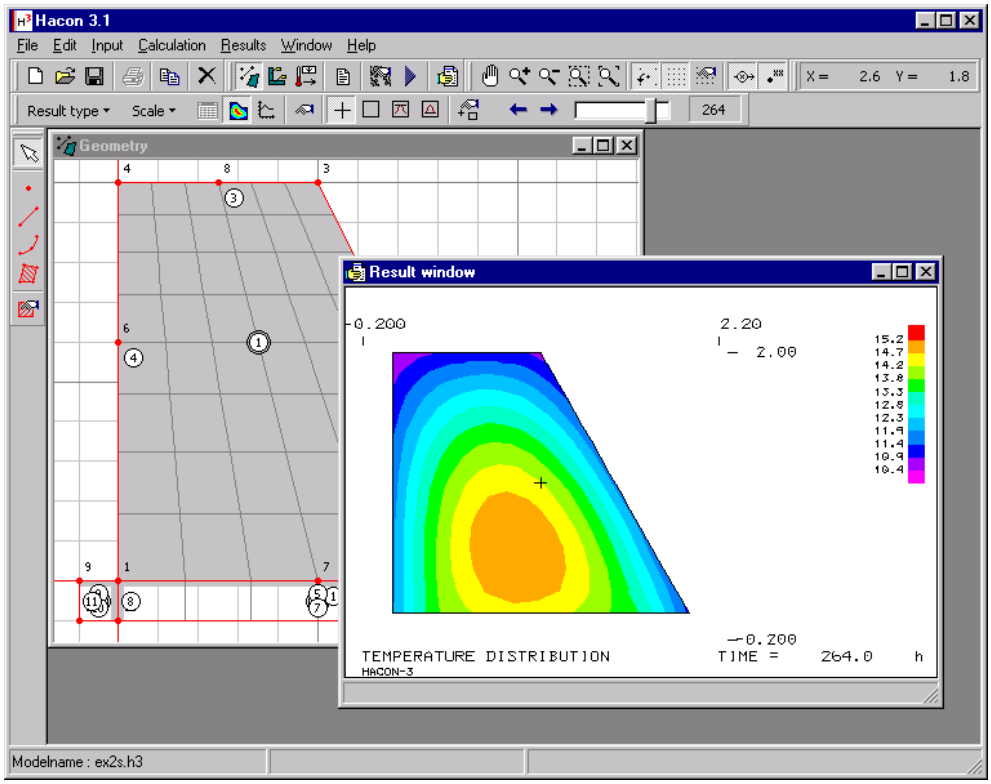

Figure 5.1: Graphical user interface to HACON

The significance of most of the data to be input is obvious. The manner of specifying the geometry may, however, need an explanation. The finite element mesh is established by a mesh generator which is based on the technique used by Liu and Chen [7]. According to this technique, the region studied is divided into a number of superelements, which are refined to finite elements by the mesh generation algorithm. The superelement mesh is established by dividing the region studied into four-sided sub-regions. A superelement where all the sides are straight is defined by the four superelement nodes at the corners.

If any of the sides of a superelement are curved, the superelement is defined by midside superelement nodes, in addition to the corner superelement nodes. The superelement node numbers have to be given counter-clockwise, starting with a corner node. In Fig. 5.2 an example of a subdivision of a region into superelements is shown. In Tab. 5.1 the corresponding data is given. In addition to the superelement node numbers, the table also shows the number of element rows and element columns the superelements are to be subdivided into. The resulting mesh is shown in Fig. 5.3. It should be noted that the numbers of rows and columns refer to a local coordinate system in a superelement and that the corner node which is given first is situated at the lower-left corner according to this local system. If a region is subdivided into rectangular superelements, it is therefore recommended that the superelement

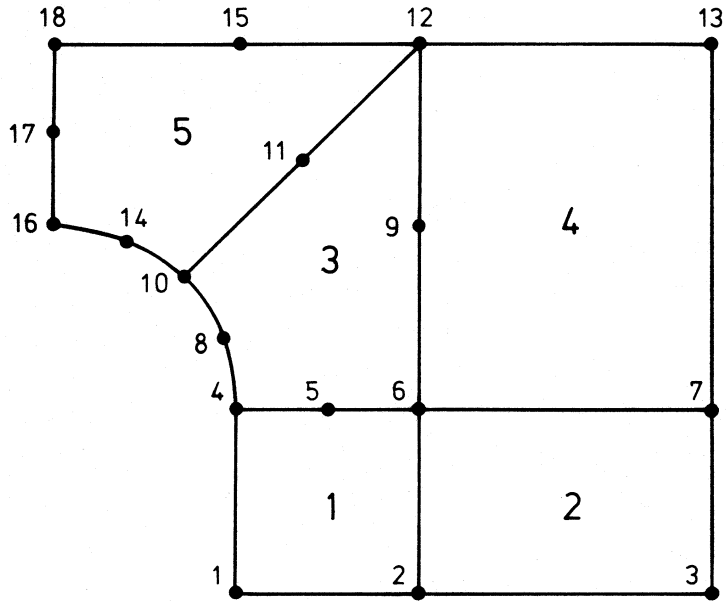

Figure 5.2: Subdivision of region into superelements.

Super-element	Superelement nodes	Number of rows	Number of columns
1	1 2 6 4	3	3
2	2 3 7 6	3	4
3	4 5 6 9 12 11 10 8	4	3
4	6 7 13 12	4	4
5	16 14 10 11 12 15 18 17	3	4

Table 5.1: Superelement data for region in Fig. 5.2.

node positioned at the lower-left corner is given as the first of the nodes defining the superelement. It should also be observed that the subdivision of two neighbouring superelements has to be the same at the common boundary.

The finite element solutions of the temperature and displacement fields will converge towards the exact solutions, as the element size is decreased. As the time step is decreased, the numerical solution procedure gives a solution which converges towards the correct one. The element size and the time step suitable for a computation depends on the problem studied and the requirements of accuracy. To find out what is suitable to use in a specific situation, one may perform computations with different element sizes, or different time steps, and study the influence on the result.

When the object studied includes an unbounded region of rock or old concrete which will be considered in the temperature modelling, superelement nodes are not positioned at the corners at infinity. Instead, superelement nodes are positioned

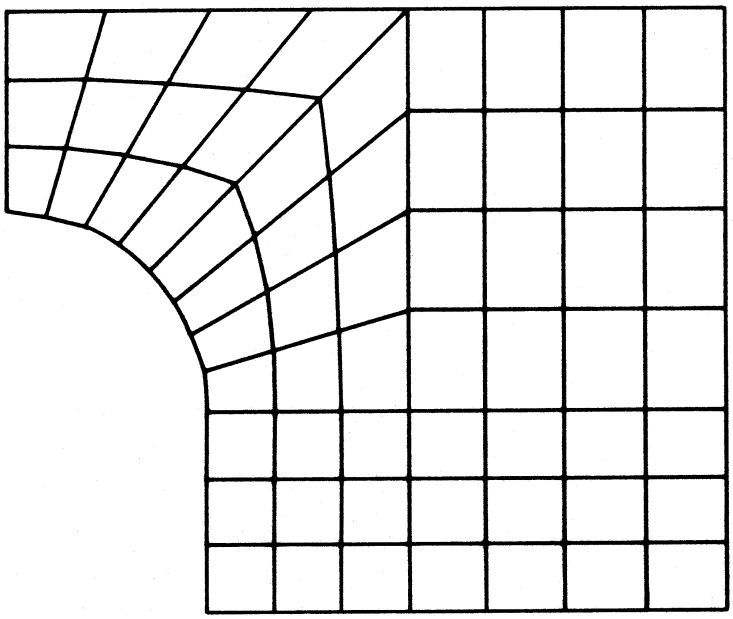

Figure 5.3: Finite element mesh resulting from the geometry in Fig. 5.2 and the data in Tab. 5.1.

where finite nodes are to be localized. The region will extend to infinity beyond these superelement nodes.

5.3 Presentation of output data

Output data is presented graphically or numerically. The program user specifies the data to be output.

The distribution of temperature at a specified time can be illustrated by colour, or by iso-lines. These images are obtained by interpolation of the nodal temperatures according to the interpolation functions in Chapter 2.

The distribution of equivalent maturity time, degree of hydration, maximum principal stress, strength and stress-strength ratio at a specified time, can be illustrated by colour. To produce these images, the value of an integration point is assumed to be representative for one quarter of a finite element, i.e. no interpolation is performed.

Principal stresses can be illustrated by arrows whose lengths are proportional to the magnitude of the stress. Displacements can be illustrated by displaying the finite element mesh with displacements multiplied by a scale factor.

The history of the temperature at a specified point and the mean, maximum, and minimum temperature in a specified region, is presented in diagrams or tables.

The history of heat loss at a specified point and in a specified region is also

presented in diagrams or tables.

The history of maximum principal stress, strength and stress-strength ratio at a specified point or in a specified region, can be presented in diagrams or tables.

Appendix A

NOTATIONS

Notations are explained in the text where they first occur. Most of them are also given in this appendix.

a_{1c}	development parameter for compressive strength
a_{1E}	development parameter for elastic modulus
a_{1t}	development parameter for tensile strength
a_{2c}	development parameter for compressive strength
a_{2E}	development parameter for elastic modulus
a_{2t}	development parameter for tensile strength
b_{1c}	development parameter for compressive strength
b_{1E}	development parameter for elastic modulus
b_{1t}	development parameter for tensile strength
b_{2c}	development parameter for compressive strength
b_{2E}	development parameter for elastic modulus
b_{2t}	development parameter for tensile strength
C	heat capacity matrix, cement content
c	specific heat
$\mathbf{D}$	material stiffness
E	elastic modulus
E_0	elastic modulus at $t_e = t_r$
E_{cn}	creep parameter
$E_{T\sigma}$	parameter for stress induced thermal strain
$\mathbf{f}$	body force
f_{c0}	compressive strength at $t_e = t_r$
f_t	tensile strength
f_{t0}	tensile strength at $t_e = t_r$
G_F	fracture energy
G_{F0}	fracture energy at $t_e = t_r$
G_s	slip modulus
G_{s0}	slip modulus at $t_e = t_r$
J	Jacobian matrix

K	conductivity, stiffness matrix
k	thermal conductivity
N	interpolation function
n	unit vector
P	heat flow matrix, load matrix
P^0	pseudo load matrix
Q	generated heat
$\mathbf{q}$	heat flow vector
q_s	heat flow into body
r_T	recoverability of thermal strain
T	temperature
$\bar{T}$	nodal temperature matrix
T_0	environmental temperature
T_r	reference temperature (293 K = 20^0C)
t	time
$\mathbf{t}$	traction
t_1	material parameter for cement
t_e	equivalent maturity time
t_r	reference time (672 h = 28 d)
$\mathbf{u}$	displacement
$\bar{u}$	nodal displacement matrix
v	weighting function
w_C	quantity of heat developed
W_{c0}	quantity of heat developed at complete hydration
w	crack width
w^s	shear displacement in crack
x_i	coordinate
α	degree of hydration
$\alpha_{1\nu}$	development parameter for Poisson's ratio
$\alpha_{2\nu}$	development parameter for Poisson's ratio
α_T	coefficient of thermal expansion
α_t	transfer coefficient
δ_{ij}	Kronecker's delta
ε	strain
ε^a	autogeneous shrinkage strain
ε^c	creep strain
ε^e	elastic strain
ε^f	fracturing strain
ε^T	thermal strain
$\varepsilon^{T\sigma}$	stress induced thermal strain
η_E	development function for elastic modulus
η_t	development function for tensile strength
θ	parameter used in time stepping procedure,

	activation energy divided by universal gas constant
θ_0	material parameter for cement
k_0	material parameter for cement
k_1	material parameter for cement
λ_1	material parameter for cement
ν	Poisson's ratio
ν_1	initial value of Poisson's ratio
ν_2	final value of Poisson's ratio
ν_{cn}	creep parameter
$\nu_{T\sigma}$	parameter for stress induced thermal strain
ρ	mass density
σ	stress
$\dot{\sigma}^0$	pseudo stress rate
τ_n	creep parameter
ϕ_0	creep parameter
ϕ_n	creep parameter
ϕ_t	creep parameter
ϕ_t'	creep parameter

Appendix B

DETERMINATION OF HEAT DEVELOPMENT PARAMETERS

B.1 Heat development in curing box

The heat developed by the concrete in an insulated curing box is partly transmitted through the wall of the box to the environment. Thus, the heat developed per volume unit and time unit Q may be expressed as the sum of the heat content in the concrete Q_i and the heat transmitted through the wall Q_e as described by e.g. Smeplass [32], i.e.

$$Q = Q_i + Q_e \tag{B.1}$$

where Q_i is given by

$$Q_i = \rho c \dot{T} \tag{B.2}$$

and Q_e depends on the properties of the curing box in question and may be assumed to be proportional to the difference between the concrete temperature T and the environmental temperatures T_e, i.e.

$$Q_e = k_1(T - T_e) \tag{B.3}$$

To obtain a value of the coefficient k_1 for the curing box used the temperature of hardened concrete may be studied. In this case the temperature is initially raised using a heat source. After this no heat is developed, i.e. $Q = 0$. This condition and Eqs. (B.1)-(B.3) yields

$$k_1 = k\rho c \tag{B.4}$$

where

$$k = -\frac{1}{T - T_e}\dot{T} \tag{B.5}$$

The data obtained from the experiment is the concrete temperature and the environmental temperature at different times. During the time from t_{i-1} to t_i the mean value of the concrete temperature, the mean value of the environmental temperature, and the time derivative of the concrete temperature are assumed to be

$$\bar{T} = \frac{1}{2}(T(t_{i-1}) + T(t_i)) \tag{B.6}$$

$$\bar{T}_e = \frac{1}{2}(T_e(t_{i-1}) + T_e(t_i)) \tag{B.7}$$

$$\dot{\bar{T}} = \frac{T(t_i) - T(t_{i-1})}{t_i - t_{i-1}} \tag{B.8}$$

respectively. A value of the coefficient k may be obtained by substituting these values into Eq. (B.5), i.e.

$$k(t_i) = -\frac{1}{\bar{T} - \bar{T}_e}\dot{\bar{T}} \tag{B.9}$$

When k is to be determined the mean value of the values $k(t_i)$ obtained at different times may be computed, i.e.

$$k = \frac{1}{n}\sum_{i=1}^{n} k(t_i) \tag{B.10}$$

Assuming the value of k has been determined, the mean value of the heat development $\bar{Q}(t_i)$ during the time from t_{i-1} to t_i may be obtained from Eqs. (B.1)-(B.3) with the temperature and its time derivative given by Eqs. (B.6)-(B.8).

According to Eq.(2.9) the total heat developed W is given by

$$W = \int_0^t Q d\tau \tag{B.11}$$

Since the mean value of Q during each time interval is obtained as described above, the integral in Eq. (B.11) may be evaluated as

$$W = \sum_{i=1}^{n} \bar{Q}(t_i)(t_i - t_{i-1}) \tag{B.12}$$

The generated heat per mass unit of cement W_e is related to W by Eq. (2.7). Thus,

$$W_c = \frac{W}{C} \tag{B.13}$$

where C is the cement content.

B.2 Determination of maturity

The equivalent maturity time is assumed to be given by Eqs. (2.4) and (2.5). Since the temperature is obtained at specific time intervals the integral of Eq. (2.4) may be evaluated as

$$t_e = \sum_{i=1}^{n} e^{\theta\left[\frac{1}{T_r}-\frac{1}{T}\right]}(t_i - t_{i-1}) \tag{B.14}$$

with

$$\theta = \theta_0 \left[\frac{T_r - T_a}{\bar{T} - T_a}\right]^{\kappa_0} \tag{B.15}$$

where $\bar{T}$ is the mean value of the concrete temperature during the time interval, according to Eq. (B.6).

If temperature data from experiments with a certain concrete mix at different casting temperatures are available, the same maturity should be obtained by Eq. (B.14) for the different data sets at each specific value of generated heat W_c. This means that the same t_e - W_c -curve should be obtained for the different data sets. The values of θ_0 and k_0 may be optimized to minimize the difference between the curves.

B.3 Determination of degree of hydration

The degree of hydration α is defined by Eq. (2.1), in which W_c is the heat developed as described by Eq. (B.13). The degree of hydration is related to the maturity t_e according to Eq. (B.14) by Eq. (2.6). The parameters λ_1, t_1 and κ_1 in Eq. (2.6) are to be determined from the experimental data. The parameter W_{c0} in Eq. (2.1) is the heat developed at complete hydration and may be determined on the basis of the heat development of the different clinker components of the cement type in question. In the absence of a proper value of W_{c0} or if complete hydration is prevented due to lack of water the value W_{c0} may be determined in order to minimize the difference between the experimentally obtained t_e - W_c -relation and Eq. (2.6). To determine the parameters λ_1, t_1 and κ_1 Eq. (2.6) may be written

$$\ln(-\ln\alpha) = \ln\lambda_1 - \kappa_1 \ln\left(\ln\left(1 + \frac{t_e}{t_1}\right)\right) \tag{B.16}$$

which is a linear relation between $\ln(-\ln(\alpha))$ and $\ln(\ln(1 + \frac{t_e}{t_1}))$. If a value of t_1 is assumed the values of $\ln(\lambda_1)$ and κ_1 may be determined from the experimental data using the method of least squares. The values of t_1 may be optimized to minimize the deviation between the experimental data and the theoretical expression given by Eq. (2.6).

The influence of the values of W_{c0} and t_1 on the deviation between experimental data and the theoretical expression is not very strong. The heat development of one

type of cement may therefore with good agreement be described by several different combinations of W_{c0}, λ_1, t_1 and κ_1.

B.4 Computer code

Computer code for determination of the parameters according to the description above has been developed. The parameters λ_1, t_1, k_1 and W_{c0} may be determined from time-temperature data obtained from an insulated curing box. If in addition the parameters θ_0 and κ_0 are to be determined at least two data sets are required. The heat loss coefficient for a curing box may also be determined from time-temperature data. The parameters λ_1, t_1, k_1 and W_{c0} may also be determined from maturity-heat data.

Determination of heat development parameters from time-temperature data requires input of mass density and specific heat of the concrete as well as cement content. In addition to this the heat loss coefficient of the curing box has to be specified. The time-temperature data has to be available on a data file where each line contains the time (s), the concrete temperature ($^\circ C$) and the environmental temperature ($^\circ C$).

Determination of the heat loss coefficient of the curing box requires input of mass density and specific heat of the concrete. The time-temperature data has to be available on a file as described above.

Determination of heat development parameters from maturity-heat data requires a data file where each line contains the maturity (s) and the heat developed (J/kg).

Bibliography

[1] Anderson, C.A.: Numerical creep analysis of structures, Chapter 8 of Creep and Shrinkage in Concrete Structures, edited by Z.P. Bazant and F.H. Wittman, John Wiley & Sons, 1982.

[2] Auperin, M., de Larrard, F., Richard, P. and Acker, P.: (Shrinkage and creep of high-strength concrete - Influence of age at loading), Annales de l'Institut Technique du Batiment et des Travaux Publics,No. 474, pp. 50-76, 1989.

[3] Bazant, Z.P.: Mathematical models for creep and shrinkage of concrete, Chapter 7 of Creep and Shrinkage in Concrete Structures, edited by Z.P. Bazant and F.H. Wittmann, John Wiley & Sons, 1982.

[4] Betonghandbok - Material (Swedish Handbook for Concrete Construction - Material), Svensk Byggtjänst, Stockholm, 1994.

[5] Byfors, J.: Plain Concrete at Early Ages, Swedish Cement and Concrete Research Institute, FO 3:80, Stockholm 1980.

[6] Carslaw, H.S. and Jaeger, J.C.: Conduction of Heat in Solids, Second edition, Oxford University Press, Oxford 1959.

[7] Dahlblom, O.: Constitutive modelling and finite element analysis of concrete structures with regard to environmental influence, Report TVSM-1004, Lund Institute of Technology, Division of Structural Mechanics, Lund 1987.

[8] Dahlblom, O.: HACON-T - A program for simulation of temperature in hardening concrete, R, D & D-report, Serial number U 1990/31, Vattenfall Utveckling AB, 1990.

[9] Dahlblom, O.: HACON-S - A program for simulation of stress in hardening concrete, Report from Vattenfall Hydro Power Genertion, Serial number H 1992/3, Vattenfall Utveckling AB, 1990.

[10] Dahlblom, O.: HACON-H - A program for determination of heat development parameters for hardening concrete, Report from Vattenfall Hydro Power Genertion, Serial number H 1992/4, Vattenfall Utveckling AB, 1990.

[11] Dahlblom, O. and Ottosen, N.S.: Smeared crack analysis using generalized fictitious crack model, Journal of Engineering Mechanics, Vol. 116, No. 1, pp. 55-76, 1990.

[12] Damjanic, F. and Owen D.R.J.: Mapped Infinite Elements in Transient Thermal Analysis, Computers and Structures, Vol. 19, No. 4. pp. 673-687, 1984.

[13] Emborg, M.: Thermal stresses in concrete structures at early ages, Report 1989:73D, Luleå University of Technology, Division of Structural Engineering, Luleå 1989.

[14] Freiesleben Hansen, P. and Pedersen, E.J.: Maturity Computer for Controlled Curing and Hardening of Concrete (in Danish), Journal of the Nordic Concrete Federation, No. 1, pp. 21-25, 1977.

[15] Hansen, T.C. and Eriksson, L.: Temperature change effect on behaviour of cement paste, mortar and concrete under load, Journal of ACI 63, pp. 489-504, 1966.

[16] Hillerborg, A.: A model for fracture analysis, Report TVBM-3005, Lund Institute of Technology, Division of Building Materials, Lund 1978.

[17] Hillerborg, A., Modéer, M. and Petersson, P-E.: Analysis of crack formation and crack growth in concrete by means of fracture mechanics and finite elements, Cement and Concrete Research, Vol. 6, pp. 773-782, 1976.

[18] Illston, J.M. and Sanders, P.D.: Characteristics and prediction of creep of saturated mortar under variable temperature, Magazine of Concrete Research, Vol. 26, No. 88, pp. 169-179, 1974.

[19] Illston, J.M. and Sanders, P.D.: The effect of temperature change upon the creep of mortar under torsional loading, Magazine of Concrete Research, Vol. 25, No. 84, pp. 136-144, 1973.

[20] Jonasson, J-E.: Slipform Construction - Calculations for Assessing Protection Against Early Freezing, Swedish Cement and Concrete Research Institute, FO 4:84, Stockholm 1985.

[21] Khoury, G.A., Grainger, B.N. and Sullivan, P.J.E.: Transient thermal strain of concrete: literature review, conditions within specimen and behaviour of individual constituents, Magazine of Concrete Research, Vol. 37, No. 132, pp. 131-144, 1985.

[22] Liu, Y. and Chen, K.: A two-dimensional mesh generator for variable order triangular and rectangular elements, Computers and Structures, Vol. 29, No. 6, pp. 1033-1053, 1988.

[23] Löfquist, B.: Temperatureffekter i hårdnande betong (Temperature effects in hardening concrete), Kungl. Vattenfallsstyrelsen, Teknisk meddelande, Serie B, Nr. 22, Stockholm 1946.

[24] Malvern, L.E.: Introduction to the Mechanics of a Continous Medium, Prentice-Hall, Englewood Cliffs, New Jersey 1969.

[25] Marques, J.M.M.C. and Owen, D.R.J.: Infinite Elements in Quasi-Static Materially Nonlinear Problems, Computers and Structures, Vol. 18, No. 4, pp. 739-751, 1984.

[26] Modéer, M.: A fracture mechanics approach to failure analysis of concrete materials, University of Lund, Division of Building Materials, Lund 1979.

[27] Ottosen, N.S. and Dahlblom, O.: Smeared crack analysis using a nonlinear fracture model for concrete, Numerical Methods for Non-Linear Problems, Vol. 3, Edited by C. Taylor, D.R.J. Owen, E. Hinton and F.B. Damjanic, Pineridge Press, pp. 363-376, 1986.

[28] Parrott, L.J.: A study of transitional thermal creep in hardened cement paste, Magazine of Concrete Research, Vol. 31, No. 107, pp. 99-103, 1979.

[29] Parrott, L.: Effect of loading at early age upon creep and relaxation of concrete. RILEM Committee 42-CEA, International report UK5, 1978.

[30] Paulay, T. and Loeber, P.S.: Shear transfer by aggregate interlock, Shear in reinforced concrete, Volume 1, Special Publications SP-42, pp. 1-15, American Concrete Institute, Detroit, Michigan 1974.

[31] Petersson, P-E.: Crack growth and development of fracture zones in plain concrete and similar materials, Report TVBM-1006, Lund Institute of Technology, Division of Building Materials, Lund 1981.

[32] Smeplass, S.: Kalor – program documentation (in Norwegian). Sintef-report STF65 A88031, Trondheim 1988.

[33] Stricklin, J.A., Haisler, W.E and von Riesemann, W.A.: Evaluation of solution procedures for material and/or geometrically nonlinear structural analysis. AIAA Journal, Vol. 11, pp. 292-299, 1973.

[34] Thelandersson, S.: Modeling of combined thermal and mechanical action in concrete, Journal of Engineering Mechanics, vol. 1123, No. 6, 1987.

[35] Täljsten, B.: Temperature development and maturity growth for Swedish Portland Cement Type II (in Swedish), Report 1987:035 E, Luleå University of Technology, Division of Structural Engineering, Luleå 1987.

[36] Zienkiewicz, O.C., Emson, C. and Bettess, P.: A Novel Boundary Infinite Element, International Journal for Numerical Methods in Engineering, Vol. 19, pp. 393-404, 1983.

[37] Zienkiewicz, O.C. and Taylor, R.L.: The Finite Element Method, Fourth Edition, Volume 1, McGraw-Hill, London 1989.

[38] Zienkiewicz, O.C. and Taylor, R.L.: The Finite Element Method, Fourth Edition, Volume 2, McGraw-Hill, London 1991.